IMPROVING 3D MODELS BY ADDING IMAGE INFORMATION

HARI KRISHNA DHONJU
March, 2012

SUPERVISORS:

Dr. Ir. S. J. Oude Elberink
Dr. M. Gerke

IMPROVING 3D MODELS BY ADDING IMAGE INFORMATION

HARI KRISHNA DHONJU
Enschede, The Netherlands, March, 2012

Thesis submitted to the Faculty of Geo-information Science and Earth Observation of the University of Twente in partial fulfilment of the requirements for the degree of Master of Science in Geo-information Science and Earth Observation.
Specialization: Geoinformatics

SUPERVISORS:

Dr. Ir. S. J. Oude Elberink
Dr. M. Gerke

THESIS ASSESSMENT BOARD:

Prof. Dr. M. G. Vosselman (chair)
Dr. Ing. F. Rottensteiner

ABSTRACT

3D building models can be used for many applications in 3D GIS environments. More attention has been paid in automatic reconstruction of these 3D building models using airborne laser scanning (ALS) in recent years. Thus reconstructed 3D models have less accuracy in outer edges (eave and gutter) than the precise intersection lines at ridges of the building roof. The reason may be either outer edges of laser segments is rather noisy or not well determined and also the quality of edges of the building model lies in order of point spacing of ALS data as they are sample ground points on earth's surface.

In contrast to ALS data, building edges are well defined in high resolution aerial images and can be determined more accurately by photogrammetric methods. This image information is used to improve the outer edges of the building roof. The improvement of the 3D building models is performed in three steps. In the first step, existence of systematic errors is checked between ALS data and image data as they are from different sensor data acquisition systems. If there exists the systematic errors, the errors are adjusted by estimating exterior orientation parameters (EOPs). In the second step, required shift value per model line is estimated by using fitting algorithm. Finally, these shift values are adjusted geometrically in 3D space considering geometry constraints of the 3D building model.

The significant systematic errors between ALS and image data are not observed. The calculated adjusted shift values are analyzed for the outer corner points and edges of the building roof. The maximum adjusted shift values of $66cm$ and $111cm$ were observed in 3D space for gutter and ridge end points respectively, and $66cm$ and $81cm$ were in 2D space. The adjusted 3D models were evaluated with external benchmark reference dataset. Improvement obtained in the planimetric accuracy varies between 6% and 18%, and between 21% and 61% for the heights of the roof plane.

The developed method improves the 3D building models assuming that the models have correct 3D roof topology and roof plane orientation. Gutter symmetry is exploited only looking at 3D model geometry. It should be extended also to consider the extracted image lines.

Keywords

Airborne laser scanning, 3D building models, aerial images, systematic errors, image information, fitting, shift estimation, geometric constraints, shift adjustment

ACKNOWLEDGEMENTS

I would like to take this ample opportunity to acknowledge the personnel and organizations that directly or indirectly involve and support me to accomplish this research.

First, I would like to express my sincere gratitude and acknowledgement with due respect to my first supervisor Dr. Ir. S. J. Oude Elberink for his guidance and supports. This research would not have been possible to go in right direction without his care, inspiration and making me to work independently. My deepest appreciation goes to my second supervisor Dr. M. Gerke for building up my confidence with his comments, feedbacks and suggestions. I gratefully appreciate both supervisors for having long discussions despite of their busy schedules.

I would like to acknowledge course director Mr. Gerrit Huurneman and course coordinator Ms Dr. Connie Blok for their advice and guidance during my study.

I would like to thank the Netherlands Government and the Netherlands organization for international cooperation in higher education (Nuffic) for granting me a scholarship to study in the Netherlands. I appreciate ISPRS for providing aerial images, airborne laser scanning data and reference dataset.

I must extend my appreciation to PhD students Emily, Adam and Biao for their help and lively discussion during my research period. I am very thankful to Uma for encouraging and providing suggestions. I am grateful to Deepak and Arun, and they deserve my acknowledgement for proof-reading of my thesis. I must to deliver my special thanks to Suna for her help, inspiration and proof-reading of my thesis.

It's my pleasure to express many thanks to my classmates for sharing fruitful 18 months together. I owe thanks and acknowledgement to Nepalese Society for making family environment during whole study period.

Finally, I would like to express my deepest gratitude to my all family members for their love, support and guidance.

TABLE OF CONTENTS

LIST OF FIGURES

LIST OF TABLES

Chapter 1
Introduction

1.1 MOTIVATION AND PROBLEM STATEMENT

3D reconstruction of buildings has numerous applications such as urban planning, visualization, environmental studies and simulation (pollution, noise), tourism, facility management, telecommunication network planning, 3D cadastre and vehicle/pedestrian navigation. Its importance is increasing in urban areas (Kaartinen et al., 2005). With increase in the capabilities of sensor data storage and handling, acquisition systems are also improving. On the other hand, the demands from the user's perspective are getting higher to produce the improved 3D building models (Oude Elberink and Vosselman, 2011).

Airborne laser scanning is one of the major acquisition systems with higher capabilities of sensor data in recent years. More attention has been paid in automatic reconstruction of 3D building models using only airborne laser scanner (lidar) data. Deriving building heights, extracting planer roof faces and ridges of the roof, and determination of roof inclination can be done more accurately from lidar data than in photogrammetry (Kaartinen et al., 2005). In this regard, Oude Elberink (2010b) observes the quality of 3D building models derived from lidar data. According to him, the quality differences in roof edges and corner points referred to a simple half hip roof with a dormer and a flat shaded adjoined to the building is described in Figure 1.1 below.

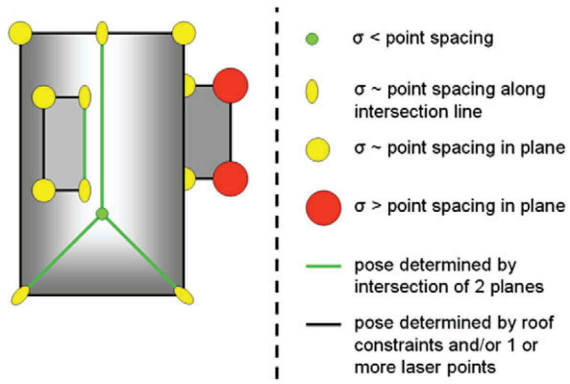

Figure 1.1: Quality differences in roof edges and corner points (Oude Elberink, 2010b).

The Figure 1.1 shows the main problem in the eave sides (outer side) of the building, have less quality than the very precise intersection lines at ridges. It may be either outer edge of laser segments is rather noisy or not well determined. And also, lidar points are sample ground points on earth's surface which implies that precise building edges can't be extracted from lidar data. Kaartinen et al. (2005) and Rottensteiner (2006) have made clear that the quality of edges of the building lies in order of point spacing of lidar data.

In contrast to lidar data, building outlines are well defined in high resolution aerial images.

The building outlines can be determined more accurately by photogrammetric methods (Kaartinen et al., 2005). This image information can be used to improve the accuracy of roof edges of the buildings of the 3D models.

As outer edges of 3D model is less accurate and the well defined building outlines can be obtained from the aerial images, We might observe some shift between model line and image line. To visualize the shift, model line can be projected in the image space and building outline can be extracted in the images. Two of the typical models are chosen to clarify observation of the shift between projected model lines and extracted image lines. Snap shots of laser points segments, building outline and projected models are depicted in Figure 1.2. When laser points are segmented for the best fit in the corresponding roof plane, eave and gutter edge side of the building outlines might not be clearly determined due to higher points spacing. The major problems seen in the eave sides are shown by yellow ellipse marking in Figures 1.2a and 1.2c. The corresponding areas in the image are shown in Figures 1.2b and 1.2d. One of possible cause might be being different in direction of laser scanning and orientation of the building outline. Higher point spacing and problem in segmentation due to the presence of higher height plane or object within the segment might be the another reason as seen in Figure 1.2c, yellow encircled gutter side of the model. Thus observed shift can be estimated and used to improve the 3D models.

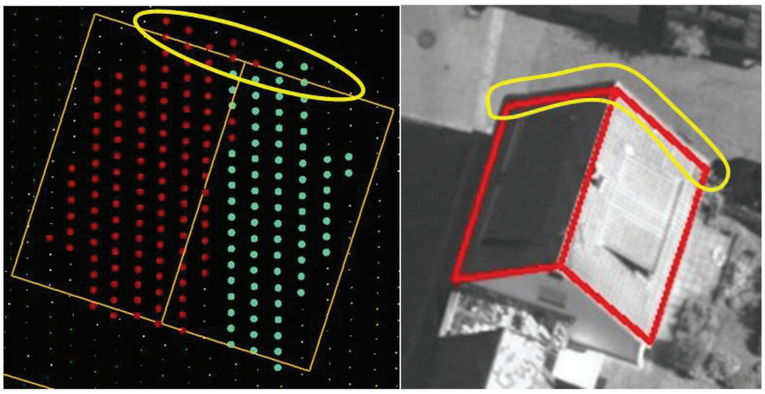

(a) Laser points for A1G1 model (b) Projected A1G1 model

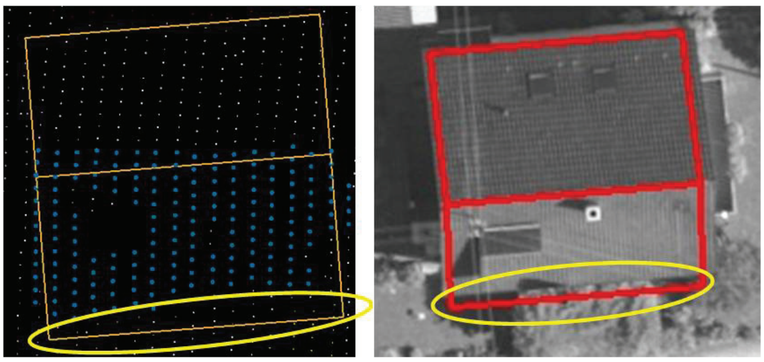

(c) Laser points for A3G11 model (d) Projected A3G11 model

Figure 1.2: Laser segments and projected models in image10050105. The yellow marking ellipses show the problem or shift between projected model lines and extreme edge of the model in the corresponding laser points segments and image.

Thus, lidar data and imagery data each has unique advantages and disadvantages. Advantages of one data can compensate for disadvantages of other data (Lee et al., 2008). Taking this into account, the accuracy can be increased as discussed above. In this context, detailed, improved and realistic 3D model of the building can be automatically reconstructed. In this consequence, this study is motivated towards developing a proper method where both information from 3D models and image information will be used to improve and to make more realistic 3D building models. Moreover, systematic errors may be observed in between lidar and imagery datasets since they are from different sensor data acquisition system. Therefore, checking the systematic errors and their adjustment is also one of the motivations of this research beforehand the building refinement processes.

1.2 RESEARCH IDENTIFICATION

As discussed in motivation and problem statement, automatically reconstructed 3D building models using lidar data have to be improved. Although, they might have well defined 3D roof type and roof topology, they have less quality in the eave and gutter sides of the building. They may not fit for certain applications as per user's perspective and demands.

On the other hand, high resolution aerial images do have well defined building outlines, color information and texture information. Taking advantage of this image information, shift between model edges and building outlines in the aerial images can be estimated by fitting algorithm. The shift values can be used to refine the eave and gutter sides of the 3D building models. Thus, this proposed research has been aimed to develop a proper method to get more improved 3D building models. Quality of 3D roof edges is also needed to evaluate for ascertaining the improvement of the 3D models.

1.2.1 Research objectives

The main objective of the proposed research is "to develop a method to improve the 3D building models by adding image information".

The research has been focused on the following sub-objectives to achieve the main objective:

- To find the match between the 3D model and image information.
- To refine the eave and gutter sides of the building using high resolution aerial images.

1.2.2 Research questions

- How to check systematic errors between lidar and image data?
- How to find the building outlines in the aerial images?
- How can the building outlines detected in aerial images be used to improve the eave and gutter sides of the 3D models?
- How can the improvement of the eave and gutter sides of the building be judged?
- Which methods should be used to test the developed algorithm?

1.2.3 Innovation aimed at

3D models are obtained from lidar data by a more data driven approach. Improving outer edges (eave and gutter) of the 3D models is the innovation of this research. Systematic errors between lidar and image data will be checked and adjusted. Then good image lines will be found to refine the outer edges of the 3D models. Improving the 3D models by adding image information is a new research in the field of Geo-information.

1.3 THESIS OUTLINE

Chapter 1: Introduction

This chapter covers motivation and problem statement, research identification, research objectives, research questions and innovation aimed at.

Chapter 2: Literature review

This chapter covers the concepts needed for this research and review on literatures. Essentially, co-registration of lidar and image data, data integration, building construction processes and 3D model accuracies are dealt . An overview on literature review is also presented.

Chapter 3: Research methodology

This chapter deals with all about the developed methodology. It covers preprocessing needed before actual refinement of the 3D models. The method for shift estimation and shift adjustment to the 3D models are discussed in the building refinement section.

Chapter 4: Experimental results and discussion

In this chapter, the study area and used data sets are dealt. Then the chapter elaborates to the experimental results and discussion.

Chapter 5: Conclusion and recommendations

This chapter is the final chapter of the thesis. Conclusion of the research, answers to the research questions and recommendations on the study are discussed.

Chapter 2

Literature review

The main aim and motive of this chapter is to acquire theoretical background needed for this thesis. It starts with co-registration of lidar and image data (Section 2.1) and data integration (Section 2.2) for checking the systematic errors between them. Then it compasses building construction (Section 2.3) in which we discuss about building construction processes, 3D models, accuracy of 3D models, edge extraction, edge matching, fitting algorithms and geometrical constraints. Finally, we present conclusion on the literature review (Section 2.4).

2.1 CO-REGISTRATION OF LIDAR AND IMAGE DATA

Data sets from different sources (sensors or platforms) can be integrated at different levels. The levels may be data level, feature level and object level (Csathó et al., 1999). Before integration, the data sets should be co-registered in the same coordinates system. Both lidar and image data are from different sources and therefore, they should be co-registered in the same framework i.e., in one coordinates system.

Several studies on co-registration can be found in literature (Stamos and Allen, 2000; Habib et al., 2002; Wang and Tseng, 2002). Stamos and Allen (2000) used 3D and 2D linear features to register the lidar data and image data using known exterior orientation parameters (EOPs). Habib et al. (2002) used 2D features to obtain EOPs using a Modified Iterated Hough Transform (MIFT) technique instead of space intersection as used by (Stamos and Allen, 2000; Habib et al., 2002). Wang and Tseng (2002) proposed a fitting method to estimate the EOPs in which line segments are used as control lines. Then these control lines are projected in the images using an approximate EOPs, and fitted to the extracted image edge pixels by changing the values of EOPs. It is noteworthy that in all methods, straight line segments are used as the control features to estimate the EOPs.

2.2 DATA INTEGRATION

Several researchers have contributed for reconstruction of 3D building models. They have proposed various approaches to explore the synergy between lidar and photogrammetric data. Baltsavias (1999) reported lidar and photogrammetry are two technologies and complementary to each other. The integration of both technologies can lead to more accurate and complete products. Vosselman (2002) combined lidar, plan view, and high-resolution aerial image data to reconstruct 3D building automatically. He described a methodology to refine 3D building roof using photogrammetric data. Plan view is used as a reference to extract the building outline from lidar data and high-resolution images are used to refine roof edge boundaries. Brenner (2004) also expressed combination of aerial photogrammetry and laser scanning can be used to produce accurate 3D building models with higher degree of automation. Lee et al. (2008) presented new approach to detect and describe complex buildings by using lidar data and aerial images. They combine the information from lidar and photogrammetric data to extract accurate building region. Intensity and height information from lidar data, and texture and boundary information from photogrammetric imagery are used to improve accuracy. This shows how to integrate both data for accurate building reconstruction, is an important and active research.

Lidar data has higher vertical than horizontal accuracy (Baltsavias, 1999). It has no texture information and difficult to extract accurate sharp boundaries of buildings solely using lidar data. Generally aerial images have higher horizontal accuracy than the lidar data (Ackermann, 1999). It can provide plenty of texture and structure information about buildings. Thereby accurate edges can be extracted from imagery data. Thus, lidar data and aerial images can be used to take advantages of both height information and image context information.

2.3 BUILDING CONSTRUCTION

Ma (2004) presented a methodology for building model reconstruction form lidar data and aerial photographs. He used lidar data with $1pt/m^2$ point density and aerial images with $0.3m$ of ground resolution. He discussed building detection, 3D building reconstruction from polyhedral model and an approach for building refinement through integration of lidar data and imagery data. He focused on refining the building geometry rather than its topology. He concluded the refinement using image information can improve 3D models reconstructed from lidar data. Dal Poz et al. (2009) also proposed a methodology for geometric refinement of 3D roof obtained from lidar data. Standard image processing algorithm is used for straight line extraction in imagery. MRF (Markov Random Field) (Li, 1994) model is used for grouping of extracted straight lines. Then the straight line groupings are back projected into lidar space to get refined building 3D roof models. They conclude most sides of the refined polygon using image building outline as the reference are better than lidar geometry.

Oude Elberink (2010a) described an automatic reconstruction of 3D building models using lidar and topographic maps in his PhD thesis. According to him, 3D building models with dormers can be constructed using only by lidar data. And he argues that the edges of the roof are of less quality than the very precise intersection lines at the roof ridges even if they have 3D roof type and accurate roof topology. The reconstructed 3D models also lacks from roof texture and small structure like chimney.

2.3.1 3D models

In real world, buildings have a numerous forms. They can be classified into two broad categories, parametric and generic model, based on the studies on building constructions (Förstner, 1999; Maas and Vosselman, 1999). Methods for building model reconstruction are normally classified as model-driven and data-driven. The model-driven or top-down approach deals with parametric building models in which extraction of low-level features is followed by use of building model knowledge. And the data-driven or bottom-up approach deals with generic models in which low-level features like points, edges and faces from image or lidar data are used.

Boundary representation (B-rep) and Constructive Solid Geometry (CSG) are two common building representation methods. The B-rep is in an assumption that the 3D building model can be represented by its bounding faces. The faces are constructed by vertices, edges and topological relations of all involving features. The CSG method is to represent the complex building models which are formed by aggregation of a set of simple primitive models.

In this study, 3D models are automatically reconstructed from lidar data using a target based graph matching algorithm from a more data driven approach as explained in (Oude Elberink and Vosselman, 2009). The work flow of the algorithm is that roof segments are extracted from laser point cloud. Then the segments are converted to planer faces using surface growing algorithm.

The topological relation between the neighboring segments are stored in a topology graph and is matched with a limited number of target graphs of the most common roof types. The algorithm is known as the target based graph matching algorithm. Then the 3D models are reconstructed by a more data driven approach although the 3D models can be reconstructed either by a more data or a model driven or a combination of both (Oude Elberink, 2009). Thus reconstructed 3D models have less accuracy in the eave sides of building (Oude Elberink, 2010b). The 3D models are needed to investigate for refining the eave sides of the building such that the model features are fitted to the image features.

2.3.2 Accuracy of the 3D models

Before discussing about the accuracy of the 3D models, it is essential to know how the 3D models are constructed. The 3D building models are automatically constructed from lidar data using the target based graph matching as described in Section 2.3.1 and applicability of these 3D models varies from user to user for the certain applications. According to Oude Elberink (2010a), the accuracy of the 3D models depends on the quality of the input data and their processing. Oude Elberink and Vosselman (2011) describe the quality of input data and three important elements of raw laser data (the accuracy of laser point clouds, the laser point cloud density and the data gaps in laser data). These can influence the quality of the target graph matching because the target graphs are created based on topological relation between the laser segments and the errors occurred in segmentation process due to highly varying point density may disturb topological relation between the segments. Subsequently, the quality of the input data and their processing impacts the accuracy of the 3D models.

Moreover, the accuracy of the 3D models also depends on geometric quality of data features. Oude Elberink and Vosselman (2011) report the geometric quality of the data features can be analyzed in two different ways, error modelling of features and empirical quality of features. The first one describes about determination of the precise specific features from lidar data using certain modeling strategy. The second one describes how the differences between the input data and extracted features are examined and analyzed.

Here, the first one is more intuitive than the second one in this study. Basically, roof faces and boundaries of roof faces are the major parts of the building constructions. The roof faces are modelled by fitting the planner laser segments and the accuracy of orientation of plane increases by its segments's size and planarity. The accuracy of boundaries of roof faces are more deeply discussed in (Oude Elberink, 2010b). The systematic overview of the problems and varying quality of edges and corner points are shown in Figure 1.1. The figure shows that the main problems are in the eave sides of the building and they have less quality than the very precise intersection lines at the ridge of the building.

A method for quality assessment of 3D building data is described in (Akca et al., 2008). In this method, input 3D model data is co-registered to the verification data by using Least Squares 3D surface matching (LS3D) method. The method is rigorous for the matching of overlapping 3D surfaces. The work flow of the method is, it estimates 7-parameters of the 3D similarity transformation of the 3D surface with respect to a template surface generated from lidar data by minimizing the sum of the squares of the Euclidean distances between the surfaces. The method describes about the reference system accuracy, positional accuracy and completeness of the building parts but not delineating of edges.

Evaluation of reconstructed 3D building models is lucidly described in (Rutzinger et al., 2009). Detail interpretation of evaluation results is explained in (Rottensteiner, 2011). The main focus is given on the evaluation of quality of the roof segmentation, topology and the geometrical accuracy of the roof polygons.

2.3.3 Edge extraction

From previous sections 2.3.1 and 2.3.2, it is clear that the 3D geometric description of the 3D models are obtained but they have less accuracy in the eave sides of the 3D building model. To refine the 3D building models, more precise outlines from other source are needed. Well defined building outlines, color information and texture information are some of the typical information that can be obtained from aerial images. Building outlines can be extracted by line detector algorithm like (Burns et al., 1986) and line-growing (Förstner, 1994) on a gradient image. These building outlines can be used to refine the 3D models. The line extracting control parameters used in the line-growing algorithm are window size for gradient calculation with the modified Roberts operator, minimum gradient threshold, minimum line length and maximum line width.

2.3.4 Edge matching

For refining the 3D models, the projected and extracted edges are needed to be matched. The matching algorithm uses different matching constraints as well explained in (Zlatanova and van den Heuvel, 2002). The main three constraints can be described as, the first one is an angle between projected and extracted edge. This constraints helps to filter out outlying the candidates based on the adopted angle threshold. The second one is the buffer which can be explained as the distance between projected and detected edges. The matching algorithm looks for the matching candidates within the predefined rectangular buffer around the projected edge. And the third constraints is the length of matching edges, i. e., the minimum overlap ratio between the edges. Best edge candidates for the matching of the projected edge can be selected applying all these constraints. A picturesque of these thresholds are shown in Figure 2.1.

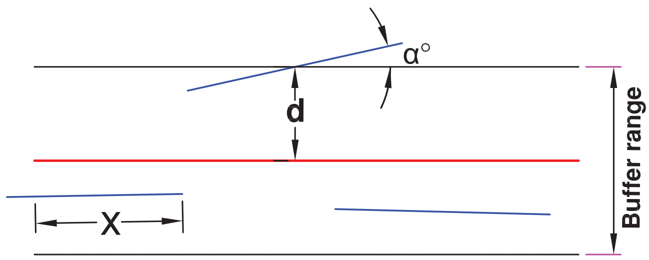

Figure 2.1: Match line parameters viz α : angle, d: Distance or buffer and x: minimum overlap between the edges thesholds. Red line is projected model edge and blue lines are image edges

2.3.5 Fitting algorithms

If an approximate model alignment from lidar data and well-defined building outlines from aerial image data of the 3D model are known, more precise building parameters can be estimated by fitting the 3D model to the images. Several approaches can be found in the literatures to optimize the alignment of the object model by the fitting.

Sester and Förstner (1989) use a probabilistic clustering algorithm to find the approximate location of the projected model in the image. Then robust estimation is done to get the final result. Both algorithms work under finding the correspondences between the project model edges and extracted image edges. The robust estimation is applied for measuring polyhedral objects whereas the the probabilistic clustering method is limited to find few number of parameters.

Lowe (1991) uses a *least square fitting* approach to fit the edges of the projected wire frame to the edge pixels. The edge pixels are the pixels with a grey value gradient above some preset threshold. This method works with the minimization of the square sum of perpendicular distances between the edge pixels and the nearest wire frame edge. It is an iterative least square method which approximates the change in parameter's value to minimize the square sum of these distances.

Fua (1996) describes fitting of a polyhedral object model to an image by *snake* approach. He explains that the model's state variable can be adjusted by minimizing the value of objective function nearly to satisfy all constraints. As a result, a good model of the object can be obtained. This compromises to refine the model with increase in accuracy as well as the consistency of the reconstruction.

Vosselman (1998) modifies the Lowe's algorithm. Lowe has given an equal unit weight for each edge pixel. Instead of using only the edge pixels in the fitting algorithm by Lowe (1991), Vosselman has created a buffer around the projected wire frame edge then use of all the pixels within that buffer. To ensure to the pixels with higher gradients dominate the parameter estimation, the algorithm uses squared grayed value gradient of the pixels as weight in the observation equation. The observation equation for each pixel is expressed as in equation 2.1.

$$E(\triangle u) = \sum_{i=1}^{i=K} \frac{\partial u}{\partial p_i} \triangle p_i \tag{2.1}$$

The weights to observation equations are given by the equation 2.2.

$$W(\triangle u) = \left\{ \frac{\partial g}{\partial u} \right\}^2 \tag{2.2}$$

Where,

$\triangle u =$ the perpendicular distance of a participating pixel to its nearest edge of the wire frame

$p_i =$ the object parameters

$K =$ the number of parameters

$\triangle p_i =$ the approximate change in i^{th} parameter to be found out

$g =$ the pixel intensity

$\frac{\partial u}{\partial p} =$ the partial derivative of the distance with respect to the specific parameter.

$\frac{\partial g}{\partial u} =$ the partial derivative of the gray value g in the direction of u perpendicular to the edge of the wire frame.

The fitting algorithm used by Fua (1996) needs a number of iteration to obtain the best parameters, which is computationally expensive. The reason is that the gray gradients show the direction where parameter values has to be changed. In terms of convergence of the least square fitting algorithm, the approaches used by Sester and Förstner (1989); Lowe (1991) computationally faster. In this fitting algorithm, if gray gradient values are below the threshold values, the weak edge pixels do not participate in the parameter estimation. Whereas, all pixels do participate within a buffer for the parameter estimation in Vosselman (1998) fitting algorithm. Thereby a large number of pixels involve at once and gradients influenced by the background objects with perpendicular direction do not interfere to the parameter estimation.

In contrast to the fitting algorithms used by Lowe (1991) and Vosselman (1998), Panday (2011) describes differently by using only n^{th} pixels along the extracted image edge for the parameter estimation. Whereas Lowe (1991) uses all pixels of the edge and Vosselman (1998) uses all pixels within a buffer around the projected model edge. Specifically, the algorithm is used for the linear features only, which suffices adequate observations to make the algorithm robust and faster. The algorithm gives an equal weights to the pixels similar to Lowe (1991).

2.3.6 Geometrical constraints

The 3D model can provide additional information like the geometrical constraints. An overview of different type of constraints are given in (van den Heuvel and Vosselman, 1997). Coplanarity, parallelism, perpendicularity, symmetry and distance ratio are the most common constraints. The geometric constraints are broadly categorized into two groups. First is topology constraints and the second is object or model constraints (van den Heuvel, 1998).

The topology constraints results from topological relations of the object topology itself. The topology constraints ensure relation between geometrical elements, the coplanarity of the object faces and a valid boundary representation of the object model.The geometry object constraints are additional information based on the geometry of the object. They represent geometric object information of the model lines or planes such as coplanarity of lines, parallelism, perpendicularity and symmetry. These constraints can be additional information in the building refinement processes.

2.4 LITERATURE REVIEW: CONCLUSION

Improving 3D models derived from lidar data using image information is a process of data integration. In which two sources of data (laser scanning and photogrammetry) are used. As we have already discussed in the previous sections 2.1 and 2.2 lidar data and image data need to be coregistered for the data integration. For co-registration purpose, lidar coordinates is taken as the basis of co-registration. The ridge edges from the 3D models can be used as control features. Based on these control features, EOPs values can be estimated as explained by Wang and Tseng (2002) for co-registration of lidar and image datasets. Then we can proceed for 3D building refinement processes.

3D models used in this study are constructed using ALS point cloud by indentifying the building points from a coarse building map. These building points are segmented by a plane based surface growing method. Roof plane topology is matched against predefined primitive roof models from a library database. Then the 3D models are constructed by a more data driven approach (Oude Elberink and Vosselman, 2009). In these 3D models, the accuracy of models' edges varies from each other. Outer edges (gutter and eave sides) of the models are less accurate than the intersected edge at ridges or interior roof edges of the model. The reason may be either outer edges of laser segments is rather noisy or not well determined and also the quality of edges of the building model lies in order of point spacing of ALS data as they are sample ground points on earth's surface..

Line features can be more precisely determined in the images. If we could add this information with 3D model lines, we can get improved and accurate 3D models. we can estimate shift between image line and model line using fitting algorithm and then adjust the model using geometric constraints of the model. Discussion on the general geometric constraints can be found in (van den Heuvel and Vosselman, 1997) and (van den Heuvel, 1998). However, additional specific constraints may require to maintain models' geometry shape and topology. The additional specific constraints might be eave adjacency constraints, gutter adjacency constraints and gutter symmetry about its ridge. These constraints need to be exploited to obtain improved 3D models without disturbing its geometry shape and topology.

Chapter 3

Research methodology

This chapter discusses a step by step explanation of each process adopted in this research. Preprocessing that should be under taken before doing actual building refinement process, is described in the Section 3.1. Each step under taken in building model refinement process is discussed in the section 3.2. Figure 3.1 shows overall methodology adopted in this research.

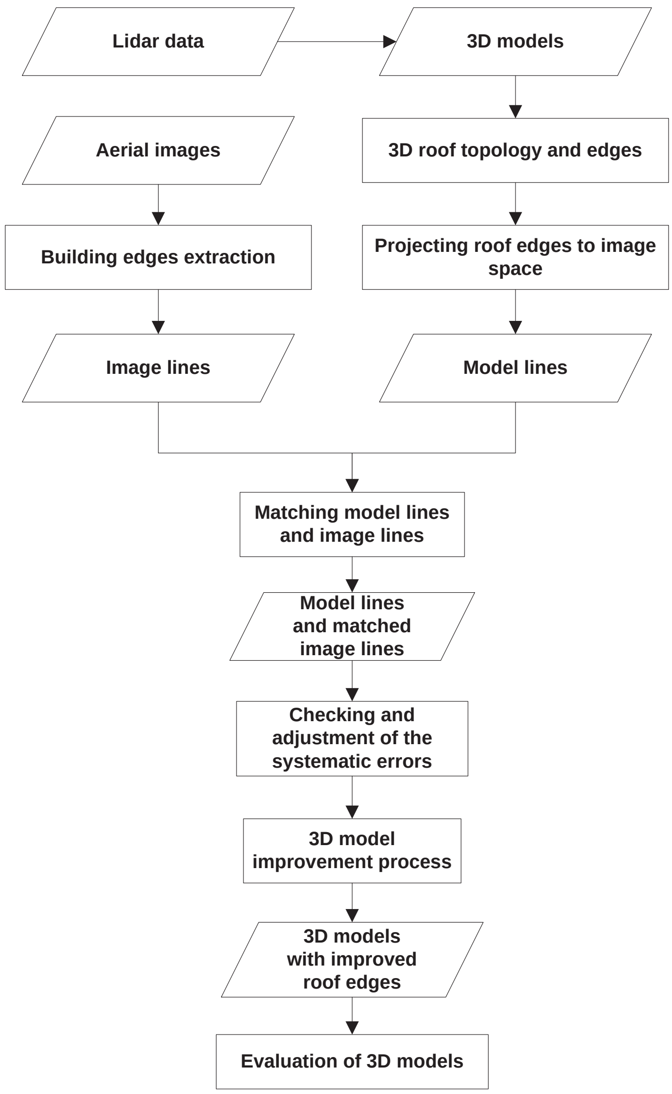

Figure 3.1: Adopted methodology

3.1 PREPROCESSING

Lidar and image are the main two data sets used in this study. They need to be co-registered in the same coordinates system for the actual refinement of the eave sides of the 3D models. The data sets may contain systematic errors even if both data sets are in the same coordinate system as they are from different sensors or platforms. Therefore, it is necessary to check whether there are systematic errors between them or not. As lidar data are explicitly in a 3D coordinates system, it is convenient to take the coordinates system of the lidar data as the common framework. If the systematic errors do exist, exterior orientation parameters (EOPs) are corrected by adjusting the systematic errors for the aerial imagery with reference to the lidar data. Where, EOPs are the position of the exposure center (X_0, Y_0, Z_0) and camera pose (ω, ϕ, κ). The EOPs can be estimated and checked by the Least-Squares Model-Image Fitting (LSMIF) (Wang and Tseng, 2002). Thereupon, the systematic errors are adjusted. Then, the data sets will be ready for the actual refinement of the eave sides of the 3D model.

3.1.1 Checking systematic errors

Linear features such as precisely intersected ridge lines of the 3D models from the lidar data are separated. These model lines are projected based on well known collinearity equations to the image coordinates system using the known EOPs. Image lines are extracted as described in Section 2.3.3. Thereafter referring Section 2.3.4, the projected model lines are matched to find the corresponding image lines in the image. The perpendicular distances between the matched model line and the extracted image line are computed. If the perpendicular distances are found within the limit of the accuracy of the data sources(lidar and image data) then we can say that the distances are not significant. Otherwise the distances are significant. If the perpendicular distances are found significantly with specific direction, it is understood that there do exist systematic errors between the lidar data and image data. Then, these systematic errors are set to adjust by minimizing the square sum of these perpendicular distances.

3.1.2 Adjustment of the systematic errors

If there do exist the systematic errors between the lidar data and image data, it is required to adjust for exploiting the image information to improve the 3D models. To adjust these systematic errors, the EOPs are estimated. The EOPs can be computed by changing the EOPs values such that the extracted edge pixels are optimally fit to the projected model line. Least-squares Model-image Fitting (LSMIF) is used to achieve optimal fitting as purposed by Wang and Tseng (2002). The method is described below in detail.

According to Wang and Tseng (2002), a small buffer is created around each of the projected model line. The extracted image line pixels that are inside the buffer are considered as the real image line pixels and used for the least square fitting. The method can be used a bit differently as we use only the image line pixels with unit weights from the matched extracted image lines, using n^{th} pixels of the matched image line which is adequate for the EOPs estimation. Figure 3.2 shows one of the projected model line and the pixels in the matched extracted image line. The perpendicular distances between these projected model line and the pixels in the matched extracted image line, are minimized to get estimated EOPs in LSMIF model. Thereby, the systematic errors are adjusted.

In figure 3.2, the projected model line is matched with the extracted image line. The perpendicular/normal distance d_i from the extracted image line pixel to the projected model line is taken as a discrepancy as an observation which is expected to be zero. Here, main objective of the fitting

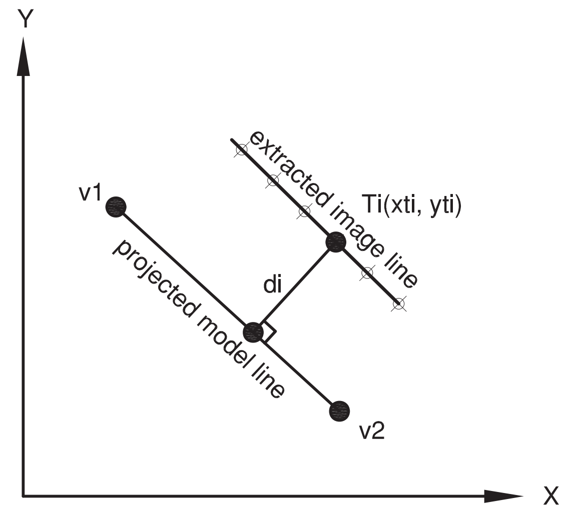

Figure 3.2: Perpendicular distance between projected model line and extracted image line

function is to minimize the distance d_i between the extracted image line pixels $p_i(x_{ti}, y_{ti})$ and the projected model line v_1v_2 by varying the values of EOPs.

Where, i is the index of the extracted image line pixels. The vertices v_1 and v_2 are the function of EOPs ($X_0, Y_0, Z_0, \omega, \phi, \kappa$). Every extracted image line pixel gives an equation. Thus, the goal of the fitting is to minimize the square sum of the distances d_i by changing the values of EOPs. Thereby image orientation parameters are determined by applying iterative least square adjustment to the fitting model function. More details on implementation of this method is described in (Wang and Tseng, 2002).

3.2 BUILDING MODEL REFINEMENT

As we discussed in the sections 2.3.1 and 2.3.2, the 3D models reconstructed using lidar data have less accuracy in eave and gutter sides of the 3D building model. To improve these outer edges of the building, characteristics of 3D model lines and image edges are needed to be investigated. For this, first 3D model lines are projected into the image(s) then image edges are extracted per model using algorithm described in the section 2.3.3. Corresponding match lines per model line are found as discussed in the Section 2.3.4. Required shift per model line to improve the model line is computed by observing the characteristics of matched image edges. An illustration of shifts in gutter and eave sides of the 3D building model are clearly described in the Figure 3.3. Finally these observed shifts are adjusted for outer edges of the model in 3D considering the geometrical constraints to get the refined 3D model.

In the shift adjustment method, specific assumptions are made based on the 3D model reconstruction lidar data. The assumptions are listed below and are carried out on the building refinement process.

- The topology of the 3D building model is correct.
- The roof planes have correct orientation.
- The gutters of the roof have same elevation.

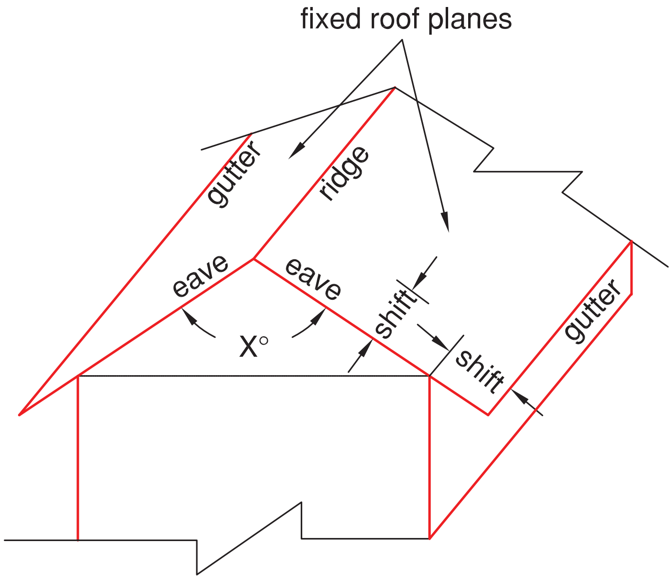

Figure 3.3: Elements of 3D roof model and required shifts to be adjusted

3.2.1 Shift estimation

It is aspired to have optimal shift per model line of the 3D model. A fitting algorithm can be used to estimate the required shift value. The algorithm fits the model line to extracted image edge(s) to get optimal shift value and works under minimizing square sum of the perpendicular distance between each pixel of the nearest image edges and model line. A linearized observation equation for each pixel is illustrated as in equation 2.1 in the section 2.3.5.

Here the model lines are the projected 3D model lines into the image(s). The image edges are the extracted linear features per building model by using line extraction algorithm Förstner (1994). Then corresponding matches between model lines and image edges are found.

Lowe (1991) uses all pixels of image edge and the equal weight for all observations concerning to the specific image edge. Vosselman (1998) considers both edge and non-edge pixel. Panday (2011) describes differently by using only n^{th} pixels giving equal weights along the extracted image edge for the parameter estimation. It is noteworthy that they all describe about model fitting to images. But we need to estimate shift value per model line rather than model fitting and the type of solution is linear. For this purpose, we use only the image edge pixels. Average gradient of pixels of model line underlying image edge is calculated differently for obtaining weight factors per image edge. From these observations and weight factors for the observations per image edge, linear solution is obtained to get the estimated shift value per model line.

The perpendicular distances between each pixel of matched extracted image edges and model line are computed as the observations. We propose different approach to calculate weight for the observations per image edge. Since we use all pixels of an image edge, longer the length of the image edge higher will be number of the observations. This will lead to give higher weight to the longer length indirectly. In addition, weight for the observations is extended by calculating standard deviation of observations per image edge, average pixel gradient of model line underlying the image edge and ratio of image edge length to the model line length. Higher value of the inverse of standard deviation gives higher weight to parallel image edge and lower weight to the more angled image edge. The average gradient of model line per image edge is used to higher weight to the strong gradient image edge. Sobel Gradient operator is used for calculating average gradient of model line underlying image edge. All these weight factors (inverse of standard deviation, average gradient of model line underlying image edge and image edge length to model line length ratio) are normalized by its own maximum value. The product of each of these weight factors is used as weight for the observations per image edge. Weight function for calculating the weight factor for the observations per image edge is given as in equation 3.1. If any one of the weight factor has become worst (weightage = 0), the equation will help to reject the edge as we use total weight as the product of each of the weight factors.

$$w = \frac{g \times lr}{\sigma} \tag{3.1}$$

Where,

σ = standard deviation of observations per image edge

g= average gradient of model line underlying image edge

lr = image edge length to model line length ratio

Using single image

Estimating the shift value per model line using single image is straight forward as discussed in the previous Section 3.2.1. In this case, 3D model lines are projected into the image space. Image edges are extracted per building model. Corresponding match of image edges per model are found. Then perpendicular distances between each pixels of matched image lines to the model line are calculated as the observations. Weight for each observations per image line is computed using equation 3.1. In the last step, linear solution is obtained for shift value per model line.

Using two images

When two image are used to estimate the shift value per model line, we need two set of observations and weights matrix i.e. one set from each of the image. Then both are combined to form a single set of observations matrix and weights matrix. Solution of the unknown shift values are estimated by solving these matrixes.

3.2.2 Shift Adjustment

Once shift value per model line is calculated, it is required to adjust in 3D without disturbing its topology. Major concern on adjustment is about eave and gutter edges of the 3D Model as we assume ridge and tilted intersection lines are the precise intersection of roof planes. Ridge and tilted intersection lines are the interior roof edges ((Oude Elberink, 2010a)). Main three constraints are considered for shift adjustment. They are adjacent eaves relationship, adjacent gutters relationship and symmetry of gutter about its ridge. Each of these constraints are discussed in details below. An illustration of 3D building roof elements and the constraints properties are shown in the Figure 3.4. Other geometrical constraints such as parallel, perpendicular, horizontal gutter and ridge elevation are carried out from input 3D model as it is. Then shifts are adjusted by roof plane extending or trimming for eave and gutter sides of the corresponding roof planes without disturbing roof plane orientation i. e., fixed roof planes. Thus geometry and topology of the 3D model are preserved even after shift adjustment is done to all outer edges(eaves and gutters) of the 3D building model.

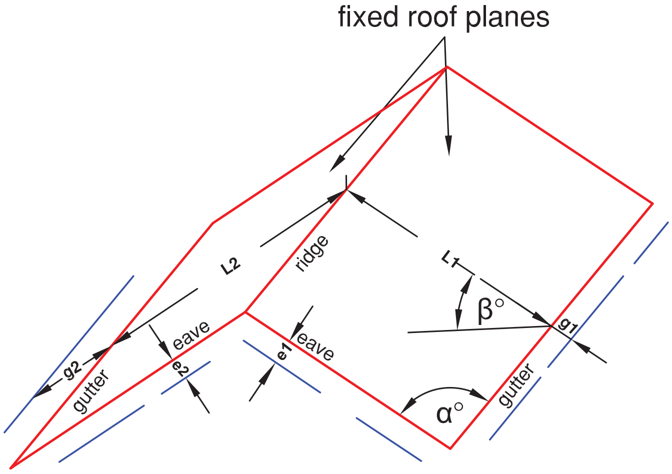

(a) Gable roof elements

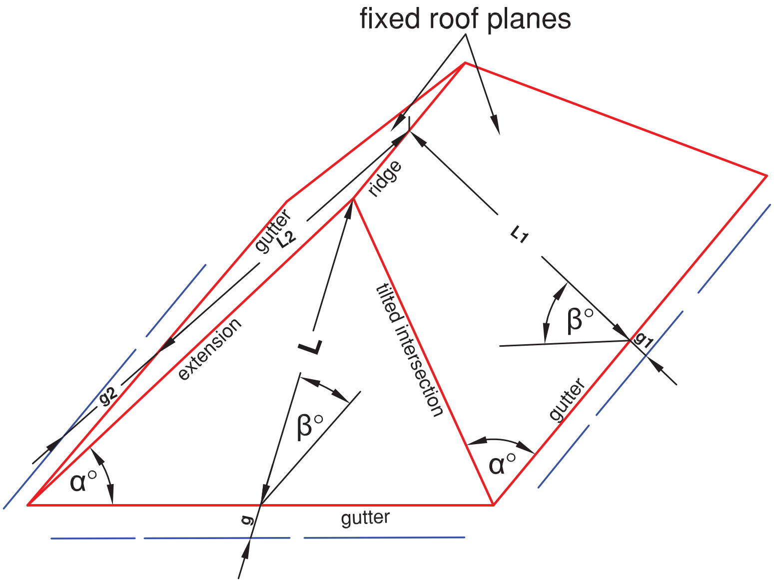

(b) Hip roof elements

Figure 3.4: Different 3D building roof elements. Where, red lines are 3D roof edges; blue lines are expected extracted image edge position; L, L1 and L2 are 3D lengths between ridge and gutter; α is an angle between two adjacent roof edges i.e. gutter and eave or intersection edge; and β is a roof inclination with respect to horizontal plane.

Eave adjacency constraint

The eave adjacency constraint means that two eave connect at the same ridge point and they are adjacent to each other. Equal shift correction should be applied for both of the adjacent eaves.

Usually, the observed shift values for adjacent eaves are differed from each other. The Figure 3.4a shows the shift value for each of the eaves. If we maintain the geometry constraints like parallelism between eave to eave and perpendicularity between eave and gutters, shift values must be equal for all adjacent eaves. If we consider two adjacent eaves for a gable roof, we can find three observation cases of shift values. First, we can find shift values for both eaves. Second, one of the eaves have shift value and other does not have due to the other eave has no any matched image edge. And the third, both of eaves have no shift values as there are no any match edges for both of the eaves. For the first case, weight value is calculated based on the maximum average gradient of the matched image edges for each eave. Then actual shift value for both of the eaves is computed using the weights as in equation 3.4. For the second case, the known shift value of the eave is used for the unknown one. And for the third case, there is no need of adjustment as there is no observed shift value for each of the eaves.

If e_1 and e_2 are two significant shift values for $eave_1$ and $eave_2$ after adjustment then equation 3.2 must be fulfilled.

$$e_1 = e_2 \tag{3.2}$$

To maintain the equation 3.2, new eave shift value is calculated using the equation 3.4.

$$grad = grad_1 + grad_2 \tag{3.3}$$

$$aes = \left(\frac{grad_1 \times e_1}{grad} + \frac{grad_2 \times e_2}{grad}\right) \times p \tag{3.4}$$

Where,

$grad_1$ = maximum of average gradients of the matched image edges for e_1.

$grad_2$ = maximum of average gradients of the matched image edges for e_2.

$grad$= total gradient and always must be greater than zero.

aes = actual eave shift value for each of the adjacent eaves.

p = pixel size of the image.

Gutter adjacency constraint

The gutter adjacency constraint means that two gutter connect at a common point and they are adjacent to each other. Equal shift correction should be applied for both of the adjacent eaves.

Similar to differ in the eave shift values, we can observe different shift values for each of the gutter edges. The Figure 3.4b shows the shift value for each of the gutters. Similar to the eave constraints, if we maintain the geometry constraints, horizontal gutter, perpendicularity between gutter and eave or intersection line, parallelism between gutter and ridge or gutter and gutter symmetry about ridge, new shift value for each of the gutter must be recalculated. For each of these cases, revised shift value is calculated. For the first three cases, revised shift values are calculated as described in eave adjacency constraints 3.2.2 and the actual shift value is calculated using the equation 3.8. For the fourth case, it is separately discussed.

If there are n adjacent gutter lines, new gutter shift value is calculated by using equation 3.7. While calculating the new gutter shift value, condition of gutter constraints must be maintained as of equation 3.5. Actual gutter shift per eave or intersection edge is calculated by equation 3.8.

$$g_1 = g_2 = \ldots = g_n \tag{3.5}$$

$$grad = \sum_{i=1}^{n} grad_i \tag{3.6}$$

$$g = \sum_{i=1}^{n} \left(\frac{grad_i \times g_i}{grad}\right) \tag{3.7}$$

$$ags_i = \frac{g_i}{\sin(\alpha)\cos(\beta)} \times p \tag{3.8}$$

Where,

$g_1, g_2, ..., g_n =$ observed gutter shifts for consecutive adjacent gutters.

$grad_i =$ maximum of average gradients of the matched image edges for g_i.

$grad$= total gradient and always must be greater than zero.

$g =$ new gutter shift value for each of the adjacent eaves.

$ags_i =$ actual gutter shift per eave or extension edge.

$\alpha =$ angle between gutter and eave or extension edge of the same roof plane.

$\beta =$ slope of the roof plane.

$p =$ pixel size of the image.

Gutter symmetry constraint

If a gutter has a ridge, it is always essential to check whether the gutter is symmetrical or not about its ridge. If two 3D distances between the ridge and two gutters are equal, it can be said that the gutters are symmetrical about its ridge. If the gutters are symmetrical about its ridge, it should be maintained even after shift adjustment. The checking of the symmetry is done as follows. 3D mid perpendicular distances between ridge and gutters are computed. If the difference between these 3D lengths are within the threshold given, the gutter is taken as symmetrical about its ridge and shift value for each of the participating gutter is revised based on the symmetry. Otherwise we consider only the gutter constraints as described in the section 3.2.2.

If g_1 and g_2 are two observed gutter shifts and L_1 and L_2 are two 3D mid perpendicular distances between ridge and gutters about a symmetrical ridge, the equation 3.9 must be fulfilled to maintain the gutter symmetry constraint. Then new gutter shifts are computed based on this condition and similar to the equations 3.6, 3.7 and 3.8 are used to calculate the actual gutter shifts for each of the gutters.

$$L_1 + g_1 = L_2 + g_2 \tag{3.9}$$

The constraints have been described taking typical examples of gable and hip roof. Flat roof is special case of gable roof which has no roof inclination (β angle). The adjustment can be performed simply considering the geometry of the flat roof by shifting roof edges in 3D space. In case of hip roof, iteration may need in the adjustment process due to gutter adjacency constraint and gutter symmetry constraint. The adjustment must be limited within the accuracy of data sources for convergence. Since we consider primitive constraints of the roof the adjustment method can be generalized for the complex roof building.

Chapter 4

Results and discussion

This chapter presents the results obtained from the methods implementation and discusses the results. Study area and datasets are explained in the Section 4.1. Calculation of the systematic errors is discussed in the Section 4.2. Edge shift estimation and edge shift adjustment are presented in the Sections 4.3 and 4.4 respectively. Then discussion on evaluation of adjusted 3D models is done in the Section 4.5. In the end Section 4.6, major observations and discussion are explained.

4.1 STUDY AREA AND DATASETS

The test dataset captured over Vaihingen in Germany is used. This dataset is a subset of data used for the test of digital aerial cameras carried out by the German Association of Photogrammetry and Remote Sensing (DGPF) (Cramer, 2010). The data set consists of Digital Aerial Images and Airborne Laser Scanner Data for three areas, area 1: Inner City, area 2: High Riser and area 3: Residential Area (ISPRS, 2012).

Digital Aerial Images: The images are 16 bit pan-sharpened colour infrared (CIR) images (flying height: $800m$, focal length: $120mm$, 65% forward overlap and 60% side overlap) with georeferencing accuracy of 1 pixel. The data set is part of the Intergraph/ZI DMC block with $8cm$ ground resolution (Cramer, 2010). The internal and exterior orientation parameters are known.

Airborne Laser Scanner Data: The data set was captured with a Lieca ALS50 system with $45°$ field of view and a mean flying height of 500 m above the ground, which has average point density of $4pts/m^2$ (Haala et al., 2010) with the average strip overlap is 30%. A digital surface model (DSM) is also available with a grid width of $25cm$ corresponds to the last pulse. The georeferencing accuracy of the ALS data is consistent with the exterior orientation of the DMC images.

Reference dataset: For the evaluation of the adjusted 3D models, benchmark reference dataset was used via the ISPRS web site (ISPRS, 2012). The reference dataset includes 2D outlines of multiple object types and also contains different types of urban development.

4.2 CALCULATION OF THE SYSTEMATIC ERRORS

4.2.1 Project model lines

Roof ridge lines of the 3D building models were taken as the control features for checking the systematic errors as they are from precise intersection of roof planes. These ridge lines were projected to the image coordinates system (image space) based on the known interior and exterior orientation parameters of the aerial images.

Number of ridge lines are 170, 24 and 70 respectively for the test area 1, area 2 and area 3. The length summary of ridge lines for each of the test areas are presented in Table 4.1. Minimum and maximum lengths are near to 9 pixels in the test area1 and 524 pixels in the test area 3. The average lengths for each of areas are 81, 161 and 155 pixels.

Table 4.1 Length of the projected model ridge lines

Length of the projected model ridge lines in pixels			
Area	Min	Max	Mean
Area1	**8.57**	485.22	81.07
Area2	45.84	312.71	161.34
Area3	13.46	**523.83**	154.89

4.2.2 Fixing line extraction parameters

Then image lines were extracted from the aerial images based on the line growing algorithm. Adjacent pixels are grouped together with similar gradient directions and fits a line through these pixels (Section 2.3.3). The control parameters used in the algorithm are the window size for gradient calculation (with the modified Roberts operator), the gradient threshold for the selecting candidate line pixels, the minimum required line length and the maximum width of a line.

For fixing and fine tuning the line extraction parameters, three set of different threshold values have been applied. The three parameters window size (3), minimum length (8) and maximum width (3) were kept constant for all cases. The minimum length (8 pixels) was fixed considering the minimum length of the model ridge line (8.57 pixels). The gradient threshold parameter was varied as 50, 100 and 1000 pixels.

The first case has the maximum number of extracted lines (27836) with the line extraction parameters whose values are 3, 50, 8 and 3 pixels respectively for window size, gradient threshold, minimum line length and maximum width of the line. These threshold values are used for the line extraction process in checking the systematic errors. Refer Table 4.2 to see the observed values for the test area1.

Table 4.2 Fixing line extraction parameters

Line extraction parameters for area1.			
Case	1	2	3
window size	**3**	3	3
gradient threshold	**50**	100	1000
min length	**8**	8	8
max width	**3**	3	3
extracted lines	**27836**	24654	13014

4.2.3 Fixing line matching parameters

To fix the line matching parameters, seven set of different thresholds values have been applied. Three parameters (parallel threshold, buffer distance threshold and minimum overlap ratio) are used for the matching process. The corresponding matches were found for each of the cases and areas. The summary table of the result has been presented in Table 4.3. The sixth case for which the maximum matches are found, is treated as the appropriate threshold values of the line matching parameters. The parameter values are 2.5°, 4 pixels and 0.01 respectively for angle, buffer and minimum overlap ratio thresholds.

Table 4.3 Model and image line matching

Fixing line matching parameters										
Case	1	2	3	4	5	**6**	7	Ridge lines	Extracted lines	Match%
angle (°)	1.5	2.5	1.5	2.5	1.5	**2.5**	2.5			
buffer (pixels)	2	2	3	3	4	**4**	4			
mo ratio	0.01	0.01	0.01	0.01	0.01	**0.01**	0.006			
match in area 1	128	134	136	148	138	**154**	154	170	27836	**91**
match in area 2	22	22	22	22	22	**22**	22	24	23226	**92**
match in area 3	66	68	66	68	66	**68**	68	70	29083	**97**

Then the corresponding matches between projected model ridge lines and extracted image lines were found based on the above sixth case matching parameters' values. Overall matching result is higher than 90% respect to the ridge lines for each of the test areas. The map plot of the matching result is shown in Figure 4.1 below.

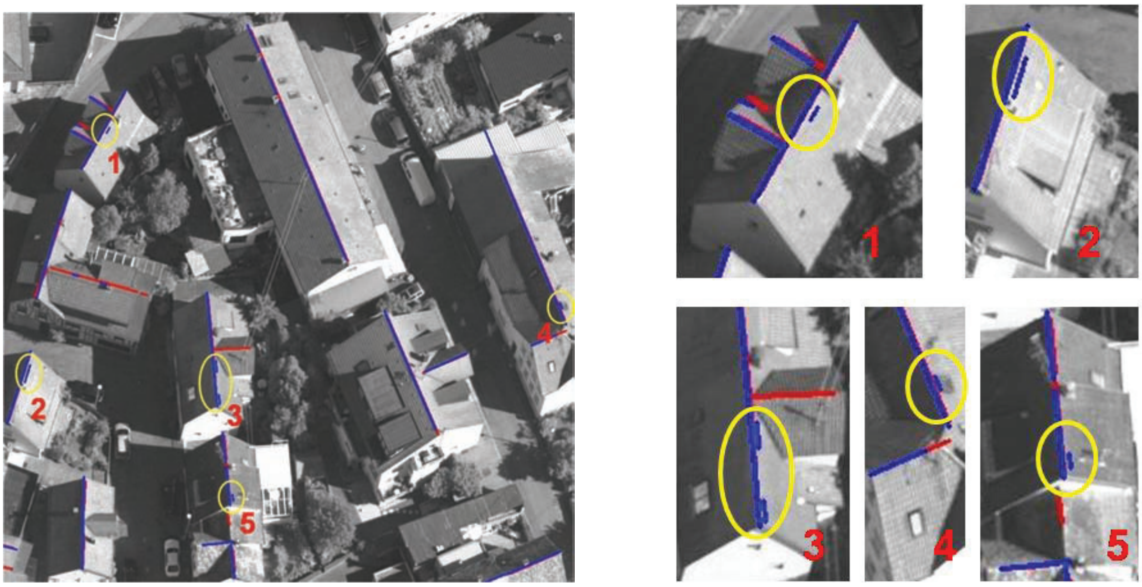

(a) Model lines and matched image lines in area 1

(b) Typical match outliers

Figure 4.1: The matching of extracted image lines to the projected model lines in the images (left). Red lines are projected model lines, blue lines are matched extracted image lines. Probable wrong match lines inside yellow ellipse marking area for the test area 1 (right)

4.2.4 Check of the Systematic errors

The image lines are extracted using the fined tuned line extraction parameters (window size: 3, gradient: 50, minimum line length: 8 and maximum width: 3 pixels) determined from Section 4.2.2. The parameters angle (2.5°), buffer (4) pixels and minimum overlap ratio (0.01) thresholds are used for line matching obtained from Section 4.2.3. Mid perpendicular distances between image lines and match lines are calculated. The distribution of these distances are found highly skewed (c.f. Figure 4.2a). Therefore median is chosen to check whether the distances are significant or not. Lower and upper limits of the median distance is calculated with 95% confidence level as explained in (Bonett and Price, 2002). The statistics of these distances and median confidence intervals are presented in Table 4.4.

Table 4.4 Statistics of mid perpendicular distances between the projected model ridge lines and the extracted image lines (in pixels)

Mid distances and median confidence intervals					
Area	Max	Mean	Med	Med $_{lower}$	Med $_{upper}$
for image10050104					
Area1	**3.8**	**1.38**	1.36	1.23	**1.48**
Area2	2.4	0.69	0.74	0.58	0.89
Area3	3.81	1.09	0.74	0.60	0.89
for image10050105					
Area1	**4.15**	**1.39**	1.31	1.20	**1.41**
Area2	2.56	0.88	0.94	0.71	1.17
Area3	3.90	1.23	0.86	0.77	0.96
for image10050106					
Area1	**4.06**	**1.45**	1.32	1.15	**1.49**
Area2	3.79	1.02	0.95	0.49	1.40
Area3	4.10	0.81	0.67	0.54	0.79

The aerial images have accuracy of 1 pixel in image orientation and 0.5 pixel in measurement. The accuracy of lidar data is also consistent with the exterior orientation of the aerial images. This produces the combined accuracy of data source is 1.5 pixels. The maximum value observed in median confidence interval is 1.49 for the test area 1 in the image1005106. Therefore it can be assumed that mid perpendicular distances are not observed significantly. Hence there is no systematic shift or errors between lidar and image data.

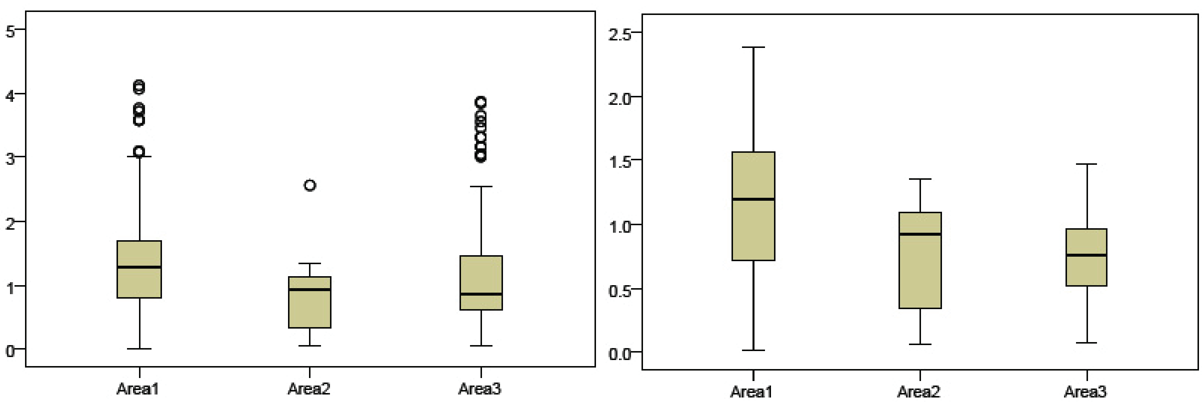

(a) With outliers (b) Without outliers

Figure 4.2: Boxplots before(left) and after(right) removal of outliers for the test area1

Check of outliers: Projected model lines and match lines are visually inspected as in the Figure 4.1. We can observe that some of the image lines are wrongly matched. The Figure 4.1b shows wrong match lines i. e., zoomed area of yellow ellipses in the Figure 4.1a for the test area 1. These wrong match lines can be treated as outliers.

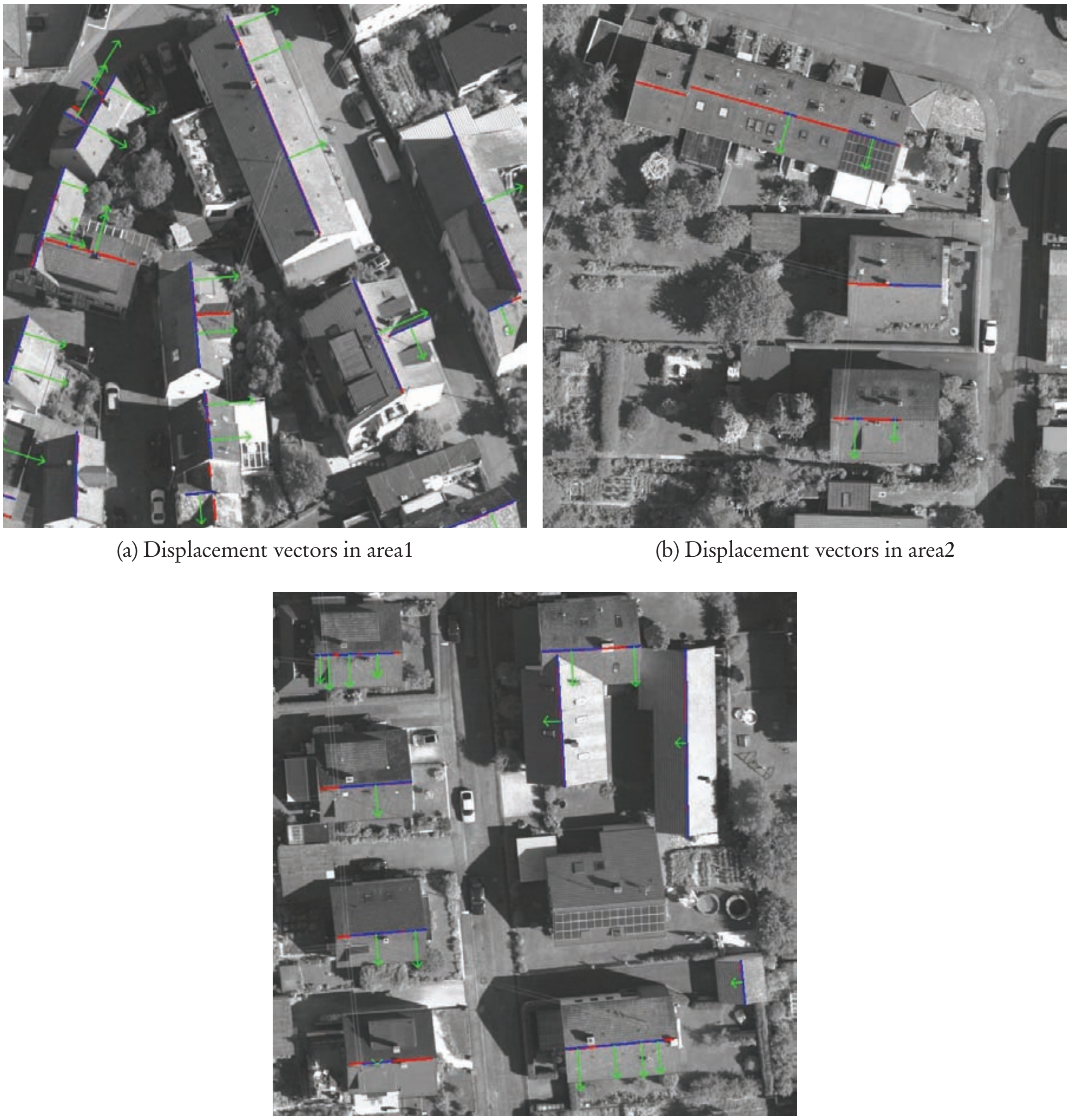

(a) Displacement vectors in area1

(b) Displacement vectors in area2

(c) Displacement vectors in area3

Figure 4.3: Displacement vectors of mid perpendicular distances between image and match lines. Red lines are projected model lines, blue lines are matched extracted image lines and green arrows are mid perpendicular distances. The arrow directions point to the model lines from the image line with mapping scale of 50.

The outliers are removed observing the boxplots of these mid perpendicular distances. Typical boxplots before and after removal of outliers are shown in Figure 4.2. The perpendicular distances are displacement vectors with direction towards model line from the image line. The map plot of the displacement vectors are shown Figure 4.3. The mapping scale for the perpendicular distance is kept 50 with respect to the model line.

To summarize, the map plots of displacement vectors have been inspected . The directions of these displacement vectors are more radial than the systematic pattern (c.f. Figure 4.3) while observing in all test areas. The maximum of median interval for the mid perpendicular distances is 1.49 pixels which is within the combined accuracy (1.5 pixels) of the data sources. Therefore, it can be assumed that there is no systematic shift or errors between lidar and image data. It is not necessary to recalculate the exterior orientation parameters of the aerial images.

4.3 EDGE SHIFT ESTIMATION

3D Model lines per building model were projected to the images using known interior and exterior orientation parameters. The image edges were extracted within ± 25 pixels extended bounding box of the building model using a line growing algorithm (Förstner, 1994). The line extraction parameters were fine tuned to get maximum number of image edges even for low contrast area. The image edges were filtered out by matching the extracted image edges with the projected model lines (Section 2.3.4). The maximum number of match lines found in gutter and eave is listed in Table 4.5. The fine tuned line extraction parameters and parameters used for filtering the image edges are summarized in Table 4.6.

Table 4.5 Maximum number of image match lines in Image10050105

Area	Gutter	Eave
area 1	19	4
area 2	11	10
area 3	36	7

Table 4.6 Parameters for line extraction and line matching algorithm (in pixels)

Line extraction		Line matching	
parameter	value	parameter	value
window size	3	parallel threshold	7 °
gradient	50	buffer size	10
minimum length	8	minimum overlap ratio	0.01
maximum width	3		

Before calculating the shift value per model line, topologically correct 28 3D building models were selected from input models. This can produce 32 models in total if two combined models are separately counted. Then, the perpendicular distance between every pixel on the image edges and the nearest model lines was taken as an observation to feed into the fitting algorithm. Weight for each observation was applied based on the weight function described in the Section 3.2.1. The weight function gives higher weight to longer, parallel and more gradient match line. Then edge shift value for each of the model lines was determined. Thus estimated shift values are in the image space. They are recalculated as discussed in the Section 3.2.1 to get actual shift per model line in 3D model space considering geometry and topological constraints of the 3D Model. Effect of number of extracted image edges or match lines per model line in the shift estimation is discussed in the Section 4.6.2.

4.4 EDGE SHIFT ADJUSTMENT

After the shift value per model line is estimated, actual shift value in 3D space is recalculated as described in the Section 3.2.2. First, if there exits eave, eave constraint is deployed to calculate required actual extending or trimming 3D length of the ridge and gutters. Then gutter symmetry about its ridge is checked and actual extending or trimming 3D length of the eave or intersection edge is calculated. Afterwards, gutter adjacency constraint described in Section 3.2.2 is deployed and final extending or trimming 3D length of outer end of eave, intersection and gutter edges are determined. Finally, new coordinates for outer ends of eave, gutter and intersection edges are computed geometrically. Subsequently, adjusted 3D building models are obtained. A typical 3D building roof models before and after adjustment are presented in Figures 4.4, 4.5 and 4.6.

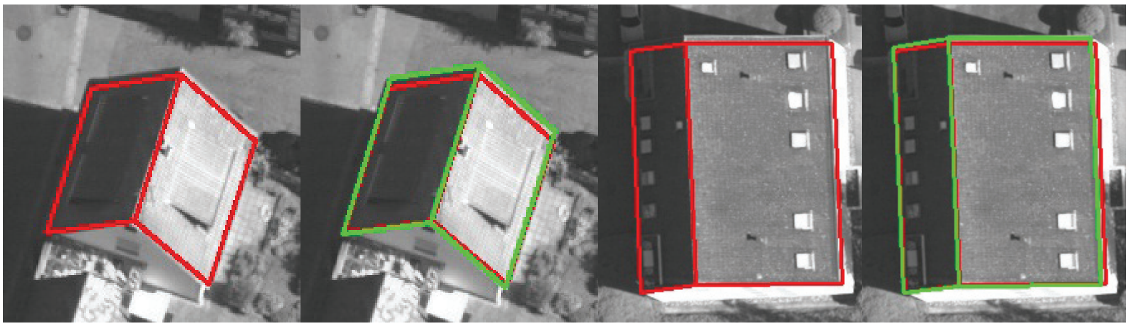

(a) Model1 of test area 1 (b) Adjusted model1 of area1 (c) Model1 of area2 (d) Adjusted model1 of area2

Figure 4.4: Building models before (left) and after (right) refinement. Red lines are projected model lines and the green lines are the adjusted model lines in image10050105.

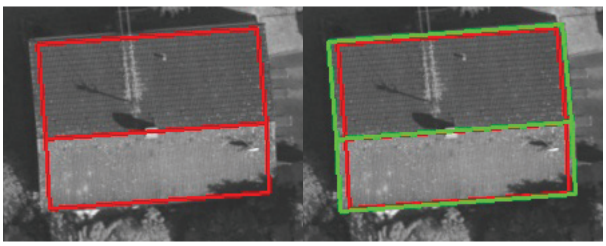

(a) Model1 of test area 3 (b) Adjusted model1 of area3

Figure 4.5: Building models before (left) and after (right) refinement. Red lines are projected model lines and the green lines are the adjusted model lines in image10050105.

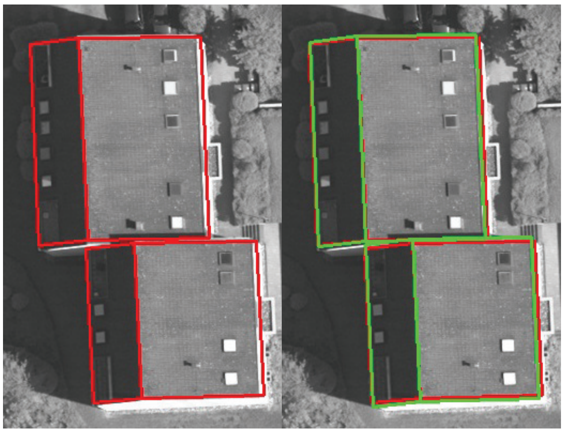

(a) Model2 of test area 2 (b) Adjusted model2 of area2

Figure 4.6: Building models before (left) and after (right) refinement. Red lines are projected model lines and the green lines are the adjusted model lines in image10050105.

4.5 EVALUATION OF ADJUSTED 3D MODELS

4.5.1 Adjusted shift

Total 28 3D building models were adjusted. Six, five and seventeen models are respectively in the test area 1, area 2 and area 3. The adjusted models were compared with input models by calculating the maximum adjusted shift values for elevation, planimetry and 3D space. The summary is presented in the Tables 4.7, 4.8 and 4.9. Overall adjusted shift values for gutter and ridge points in dz, dxy and dxyz directions are listed in the table 4.11. First character of the building model code denotes test area, second character denotes test area number and then building type(G: Gable, CH: Combined hip, H: Hip and CG: Combined Gable) followed by building model number derived from input models.

Table 4.7 Maximum adjusted shift values (in meters) for the test area 1

Model no.	dz $_{max}$	dxy $_{max}$	dxyz $_{max}$
A1G1	0.02	**0.50**	**0.50**
A1CH2	0.07	0.20	0.21
A1G25	0.09	0.36	0.37
A1H28	0.05	0.09	0.10
A1G32	0.07	0.28	0.29
A1G41	0.08	0.35	0.36
Overall max	**0.09**	**0.50**	**0.50**

In the test area1, Table 4.7 shows that adjusted shift value to the height difference (dz) of the roof is within $9cm$. The observation of adjusted shift value is $50cm$ for both planimetry and 3D space.

Table 4.8 Maximum adjusted shift values (in meters) for the test area 2

Model no.	dz $_{max}$	dxy $_{max}$	dxyz $_{max}$
A2G1	0.12	**0.39**	0.40
A2CG2	0.15	**0.39**	0.40
A2CG3	0.13	0.33	0.34
A2G4	**0.21**	0.35	**0.41**
A2CG13	0.6	0.26	0.27
Overall max	**0.21**	**0.39**	**0.41**

Referring to the Table 4.8, maximum adjusted shift value of $21cm$ is observed for height of the roof plane in the test area 2. For the planimetric and 3D space, it lies between $39cm$ and $41cm$.

Table 4.9 Minimum and maximum adjusted shift values (in meters) for the test area 3

Model no.	dz $_{max}$	dxy $_{max}$	dxyz $_{max}$
A3G1	0.08	0.58	0.58
A3G3	0.09	0.34	0.35
A3G5	0.12	0.48	0.49
A3G6	0.07	0.68	0.68
A3G7	0.05	0.50	0.50
A3CG9	0.15	0.38	0.41
A3G11	0.75	**0.81**	**1.11**
A3G12	0.22	0.28	0.36
A3G16	0.03	0.61	0.61
A3G17	0.02	0.42	0.42
A3G18	0.24	0.40	0.46
A3G21	0.01	0.21	0.21
A3G23	0.10	0.34	0.36
A3G27	0.04	0.22	0.23
A3G28	0.06	0.25	0.26
A3G29	0.03	0.13	0.13
A3G30	0.12	0.58	0.60
Overall max	0.75	**0.81**	**1.11**

Referring to the Table 4.9 for the test area 3, maximum adjusted shift value of $75cm$ is observed in height of the roof plane. $81cm$ and 111 cm are observed as the maximum adjusted shift value in planimetric and 3D space for A3G11 model. These values are separated in eave-gutter and eave-ridge points to see which points have maximum adjusted shift. Eave-gutter point is the intersection point of eave and gutter edges. Similarly, eave-ridge point is the intersection point of eave and ridge edge of the model.

Table 4.10 Range of adjusted shift values per number of 3D models for all the test areas

shift (cm)	no. of adjusted 3D models		
	dz $_{max}$	dxy $_{max}$	dxyz $_{max}$
0-10	19	1	0
10-20	6	1	2
20-30	2	7	6
30-40	0	10	6
30-50	0	4	9
50-111	1	5	5

The adjusted shift values per number of adjusted 3D building models is presented in Table 4.10. The range graph of the same table in shown in Figure 4.7. The adjusted shift range varies between $10cm$ to $111cm$. For the most of the 3D building models, the range of adjusted shift is within $10cm$ in height difference, between 30 and 40 cm in planimetry and between $30cm$ and $50cm$ in 3D roof plane.

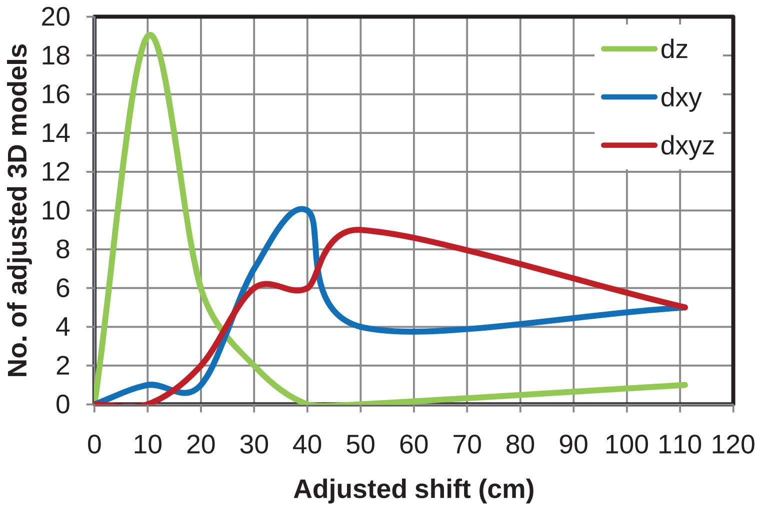

Figure 4.7: Adjusted shift per number of adjusted 3D models

Table 4.11 shows the observed minimum and maximum adjusted shift values for eave-gutter and eave-ridge points. The eave-gutter points has higher adjusted shift values than in eave-ridge points. 81 cm and 111 cm of adjusted shift values are observed respectively in planimetric and 3D space for eave-gutter points. But lower adjusted shift value of 66 cm is observed for the eave-ridge points. To illustrate it more clearly, it is visualized in the Figure 4.8. Yellow filled region represents the range of the shift value in dxyz direction. The black circles and ellipses represents the range of the shift value in dxy direction.

Table 4.11 Overall adjusted shift values (in meters) for eave-gutter and eave-ridge points.

edge	dz		dxy		dxyz	
	min	max	min	max	min	max
eave-gutter	-0.75	0.25	0.04	**0.81**	0.05	**1.11**
eave-ridge	0.00	0.00	0.00	**0.66**	0.00	**0.66**

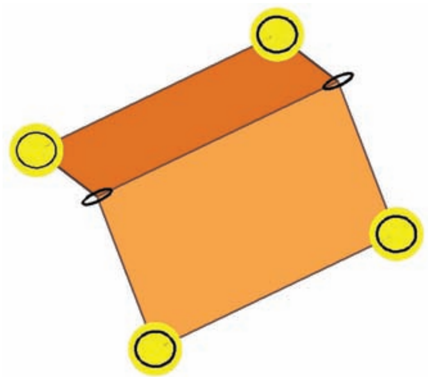

Figure 4.8: Observed range of adjusted shift in gutter, eave and ridge points.

The standard deviation of adjusted shift values in dz, dxy and dxyz direction are presented in Table 4.12 for the eave-gutter and eave-ridge points.

Table 4.12 Standard deviation values of adjusted shift values (in meters) for eave-gutter and eave-ridge points.

points	σ_z	σ_{xy}	σ_{xyz}
eave-gutter	**0.13**	0.15	**0.17**
eave-ridge	0.00	**0.16**	**0.16**

Since no adjustment is done for ridge height, the observed adjusted shift value is zero in dz direction for the eave-ridge points. The eave-gutter points have higher planimetric and 3D adjusted shift values than in the eave-ridge points (c.f. Table 4.11). Moreover, the eave-gutter points has higher variation than in eave-ridge points for dz, dxy and dxyz direction (c.f. Table 4.12). It shows eave and gutter edges are less accurate than ridge edges.

4.5.2 Evaluation with reference dataset

The adjusted 3D building roof models were evaluated to check the quality on the geometrical accuracy of the roof polygons as described by Rottensteiner et al. (2012). The topological and roof plane segmentation checking is not interest of study as both are carried out and maintained after the adjustment. The results obtained from the evaluation of the adjusted 3D building roof model is summarized in Table 4.13. The name, ITCE2 is derived from (Rottensteiner et al., 2012) and

ITCH2 is name given for adjusted 3D models. The input models are used from ITCE2 building construction approach.

The main goal of the evaluation is to check whether the adjusted 3D building models are improved or not. The work flow described by Rottensteiner et al. (2012) is as follows. It was determined the RMS errors of the planimetric distances of the adjusted roof plane boundary points to their nearest neighbor on the corresponding reference boundaries. The RMS errors in the height difference (RMSZ) were determined by comparing two synthetic DSMs generated from the 3D building models. It is based on the height differences between the reference planes and all corresponding roof planes which is also capable for including segmentation errors on the building reconstruction.

Table 4.13 Evaluation of adjusted 3D building models.

Name	RMS[m]	RMSZ[m]
Area1 (288 roof planes)		
ITCE2	0.94	0.55
ITCH2	0.77	0.39
improvement (%)	18	29
Area2 (69 roof planes)		
ITCE2	1.16	3.31
ITCH2	1.09	1.30
improvement (%)	6	61
Area3 (235 roof planes)		
ITCE2	1.04	0.42
ITCH2	0.93	0.33
improvement (%)	11	21

As we discussed in the Section 3.2, we have maintained the topology, roof plane orientation, horizontal gutter of the 3D building models on the building refinement process. Improvement can be seen looking on the Table 4.13 and varies between 6% and 18% in planimetry and between 21% and 61% in heights of the roof plane.

4.6 MAJOR OBSERVATIONS AND DISCUSSION

4.6.1 Problems in line extraction

Though line extraction parameters are fine tuned to extract as much as higher number of image lines even in low contrast area, some of the model edges could not extract as seen in the images. Typical problems in image line extractions are shown in Figures 4.9. All building outlines are not extracted in both images of the image pair, Figures 4.9a and 4.9b in the test area1. They both are needed to combine for model improvement. Similarly for the image pair, Figures 4.9c and 4.9d in the test area2 have more dangled than straight extracted lines and both needs to exploit for good model line fitting. But model in test area 3, the case is different from area 1 and area 2. In the left image (c.f. Figure 4.9e), no proper image line parallel to model line is extracted. However, in the right (c.f. Figure 4.9f), extracted image line is well defined. Thus it is needed to integrate image lines from the image pair for compensating image information.

Thus, image lines from single image may not suffice to improve the 3D building models.

Image lines form a image pair are used to solve the problems discussed above. An image pair of image10050105 and image10050106 is used for the test area 1 and area 2. For the test area 3, an image pair of image10050104 and image10050105 is used. In this case, two set of observations from each of both images are used to estimate the shift value per model line. In this way, extracted image lines from the pair images are used for compensating image information.

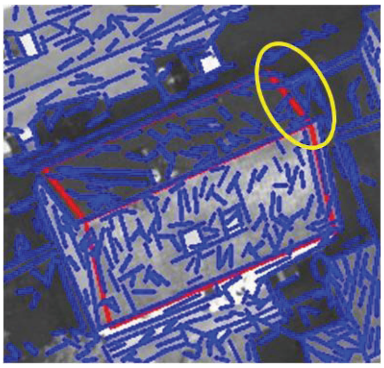

(a) A1G32 model from image10050105

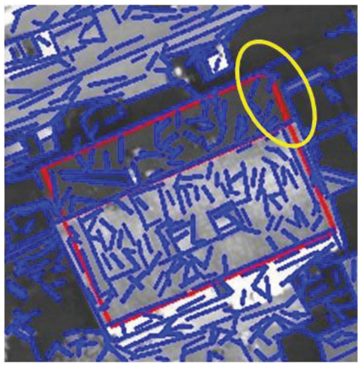

(b) A1G32 model from image10050106

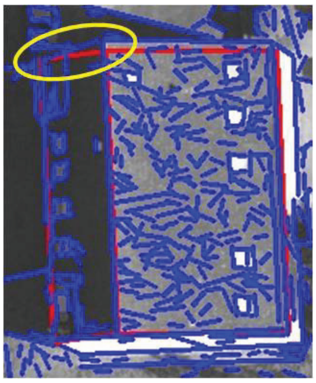

(c) A2G1 model from image10050105

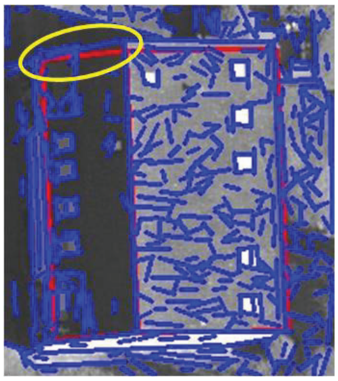

(d) A2G1 model from image10050104

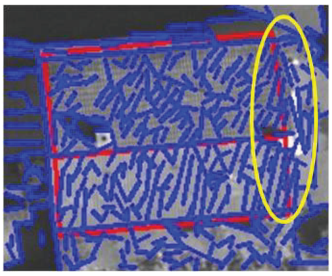

(e) A3G6 model from image10050105

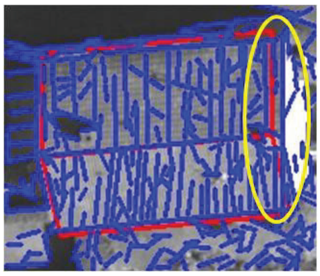

(f) A3G6 model from image10050106

Figure 4.9: Extracted image lines for the models in image10050104, image10050105 and image10050106. The yellow marking ellipses show the problems in line extraction. Extracted image lines from pair images are used for compensating image information. Left images are common for all models and right images are their corresponding pair image. Red lines are projected model lines and blue lines are extracted image lines.

4.6.2 Problems with multiple match lines

Match lines are the extracted image lines which are matched with the projected model lines. Each model line may or may not have match lines. Number of match lines are observed for the most of the model lines. For a few of the model lines, single match line is observed. One of the example is shown in Figure 4.10a. In this figure, the yellow ellipse marking area shows one of eave has number of match lines and other eave has only one match line. Since adjustment is done based on the weightage given to the match line, it fits with near to the high weighted image line. Due to this higher weightage, some model line may not fit with correct image line. The main problem might be, outer image line may have very low gradient due to low contrast of the image background than the other image lines. In contrast to the model in the Figure 4.10a, the model in Figure 4.10b has not such problem in the eave sides of the model which is shown inside the yellow ellipse marking area. Model eave lines are optimally fitted with the matched image lines.

(a) A1G32 model

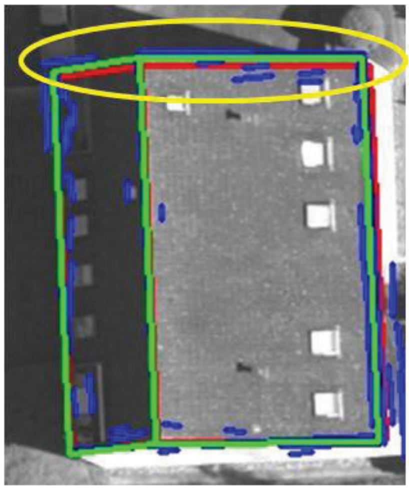

(b) A2G1 model

Figure 4.10: Multiple match lines (blue lines) in the model adjustment to the image. Green lines are adjusted model lines with matched image lines and red lines are projected model lines.

4.6.3 Model topology

For the building adjustment process, building models have to have correct topology. The topology will not change even after the adjustment. Some of the building models are also adjusted assuming that their topology is correct. Two of the building models which have incorrect roof topology are shown in Figure 4.11. The adjustment algorithm does not care about incorrectness of the roof topology, the yellow ellipse marking area and the model lines are adjusted as if the model has correct topology. This may influence on the result of 3D building model evaluation.

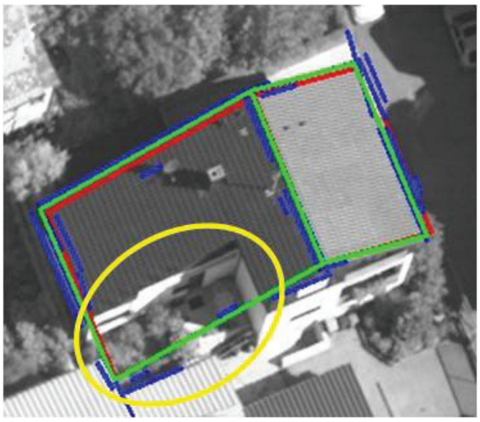

(a) A1G25 model

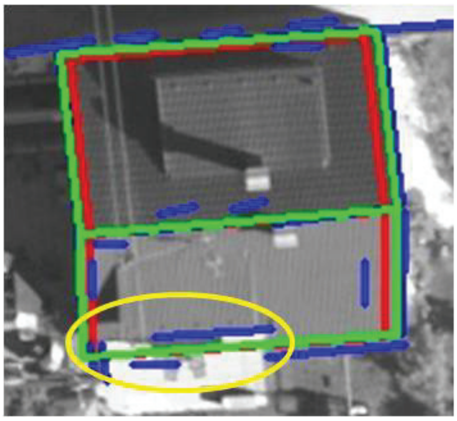

(b) A3G5 model

Figure 4.11: Incorrect topology of model roof. Yellow ellipse marking area indicates the incorrect topology. Blue lines are extracted image lines, green lines are adjusted model lines with matched image lines and red lines are projected model lines.

4.6.4 Effect of constraints

In our the method, we have employed main three constraints. They are eave adjacency constraints, gutter adjacency constraints and gutter symmetry constraints. When we add any of one of the constraints in the shift adjustment, the added constraint may affect to geometry adjustment of the model. We call this effect as the conflicts between constraints. The observed conflicts between the constraints are discussed in detail below.

Effect of eave adjacency constraint: To maintain the eave adjacency constraint, both adjacent eaves are adjusted with the same correction shift value. Referring to the Figure 4.10a in the yellow ellipse marking area, the upper eave has a good image match line which can give required shift value. The lower eave has multiple match lines. Here the effect is in between upper eave shift value and lower eave shift value. We can expect that upper eave must have better shift value than in the lower eave. But in adjustment process, we consider both eave shift values. Resultant new eave shift value is calculated and corrected for both eaves equally to maintain eave adjacency constraint. New shift value is calculated based on maximum gradient of the matched image lines. Here, the lower eave might have higher gradient value than in the upper eave and the higher preference will be given to the lower eave. The both eaves will be corrected with new shift value. The result is the eaves are not perfectly adjusted. The effect is because of the consideration of eave constraint. In contrast to the model in the Figure 4.10a, the model in Figure 4.10b has no such effect of eave adjacency constraint.

Effect of gutter symmetry constraint: Gutter symmetry is determined by calculating the 3D distances between ridge and its corresponding gutters. If the difference between these two 3D distances is within the threshold ($24cm$). Then the gutters are considered as symmetrical about their ridge. Here the constraint is the 3D distances between ridge and gutters must be equal. When this constraint is exploited, false decision may happen. Symmetrical may be unsymmetrical and vice versa. One of this case is depicted in Figure 4.12 in which model is considered as unsymmetrical though model is symmetrical based on the model geometry. This means checking the gutter symmetry based on input model is not enough. To resolve this problem, we may need to consider characteristics of longer image lines to determine the gutter symmetry.

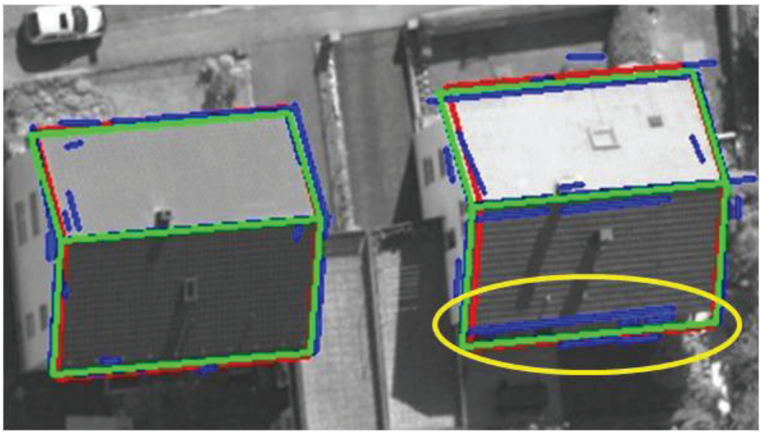

Figure 4.12: Problem seen from gutter symmetry constraint in A3CG9 model

Gutter symmetry and gutter adjacency constraint conflict: If 3D distances between ridge and gutters are equal then the gutters are considered as symmetrical. These two distances are kept equal as a gutter symmetry constraint to exploit the gutter symmetry. Adjacent gutters intersect to meet at a common point. To maintain this adjacency, the gutters are adjusted with equal shift correction. We call it as the gutter adjacency constraint.

In some of the cases, gutter symmetry may affect the gutter adjacency. If we maintain gutter symmetry we may loss gutter adjacency and vice versa. To maintain gutter symmetry, we try to make equal 3D distances between ridge and gutters. But It losses the gutter symmetry. If we try to maintain the gutter adjacency, we may loss the gutter symmetry. So we can observe a conflict between gutter symmetry and gutter adjacency conflict. In the adjustment process, if we maintain gutter symmetry about their ridge, it gives new gutter shift values. Then we deploy gutters adjacency constraints and gives also new gutter shift values, which directly affect the gutter symmetry. It makes iterative to get final adjustable gutter shift value for the gutters. To make converge the iteration, the adjustment process is limited within the accuracy of data sources.

4.6.5 Comparison of 3D building models

The input models obtained from ITCE2 building construction approach (Rottensteiner et al., 2012) and our adjusted models are performed for evaluation with the reference dataset (ISPRS, 2012). To check the improvement, both evaluation results are compared. One of the typical models before and after improvement are shown in Figure 4.13. The models are snapped from the correct buildings from the evaluation result. Figures 4.13a and Figure 4.13b are results of ITCE2 and adjusted model after evaluation. The meaning of the colours ((Rottensteiner, 2011)) is:

- **Ochre:** Pixels in buildings of which all the reconstructed roof planes have correspondences of sufficient overlap in the reference if the pixel is inside a building in both reference and reconstruction results.

- **Yellow:** Pixels in buildings of which all reconstructed roof planes have correspondences of sufficient overlap in the reference but the pixels are not inside a building in the reconstruction results.

- **Bright red:** Pixels correctly detected in roof planes that are not inside a building in the reference.

Before improvement: The area of yellow and red colors are distinctly visible in Figures 4.13a. Top edge pixels in yellow color are not inside the building in the building reconstruction results. Some of right edge pixels in red color are not inside a building in the reference.

After improvement: The yellow color pixels are decreased and the red color pixels are disappeared in Figures 4.13b. Therefore it can be seen that top edge of the building edge has been improved after adjustment. The right edge of the building has been perfectly fitted with the reference.

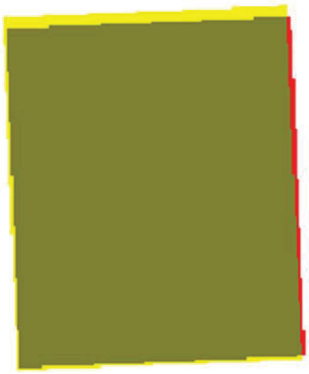

(a) A2G1 model after evaluation of ITCE2

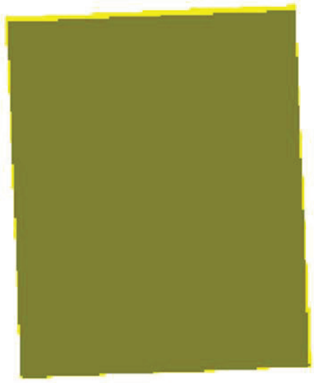

(b) A2G1 model after evaluation

Figure 4.13: Evaluation results of A2G1 model

Chapter 5
Conclusion and recommendations

This chapter describes a brief overview of the thesis in the Section 5.1, answers to the formulated research questions (Section 5.2) and some of the recommendations of this study (Section 5.3).

5.1 CONCLUSION

The main objective of this research is "to develop a method to improve the 3D building models by adding image information". 3D building models derived from lidar data are improved by adding image information from high resolution aerial images. This objective was fulfilled by three steps. First, it was checked to see whether there is systematic errors between lidar data and image data. If there exist the systematic errors, image data is co-registered with respect to lidar space. In the second step, 3D model lines are projected in the image space, image lines are extracted within an extended bounding box of projected model lines, model lines are matched to find corresponding image lines and then shift per model line is estimated by using fitting algorithm. In the last step, shift value per model line is adjusted exploiting the geometrical constraints of the model.

Three main constraints eave adjacency, gutter adjacency and gutter symmetry about its ridge are deployed. Other constraints like eave parallelism, gutter to gutter and gutter to ridge parallelism, eave to gutter perpendicularity and angle constraints between two adjacent model edges are derived and maintained from model input. Topology of the 3D building model remains same after the adjustment.

No significant systematic errors were found when checked between lidar and image data. Final adjusted 3D models were assessed by analyzing the adjusted shifts in the outer edges of the 3D models. The maximum adjusted shift values of $66cm$ and $111cm$ were observed in 3D space for gutter and ridge end points respectively, and $66cm$ and $81cm$ were in 2D space. Then the adjusted models were evaluated to check the improvement on the quality of the roof planes on the geometrical accuracy of the roof polygons rather than its topology. When looking at the evaluation results, improvement on 3D models can be achieved significantly and varied between 6% and 18% in planimetry and between 21% and 61% in the heights of the roof plane.

There are some problems in line extraction, line matching and constraints conflicts. For some of the model lines, good image lines are not extracted. Though more image lines are extracted and matched per model line, false model line fitting to the image lines is observed. Due to conflicts between eave adjacency constraints, eave side of the model is not well adjusted as expected. More study on line extraction, matched image line filtering and constraints conflict is needed for further improvement of 3D models. The study is limited for the topologically correct 3D building models.

5.2 ANSWERS TO THE RESEARCH QUESTIONS

To achieve the objective of this research, five research questions were set. The research questions and their answers are given in the succeeding paragraphs.

1. How to check systematic errors between lidar and image data?

   Roof edges of 3D building model are projected in the image space as the control features. Image lines are extracted within ± 25 pixels extended bounding box of the model. Projected roof edges and the image lines are set for matching. Mid perpendicular distance between the projected roof edges and the image lines calculated. Statistics of these distances are observed. The distribution of these distances are found highly skewed. Therefore median confidence interval is computed at 95% confidence level. The median confidence interval (upper limit of $1.49 pixels$) was found within accuracy of the data sources ($1.5 pixels$). The vectors of perpendicular distances are visually inspected and found more radial pattern. Therefore it can assumed that there is no systematic shift or errors between the lidar data and image data.

2. How to find building outlines in the aerial images?

   3D model lines are projected in the images and image lines are extracted using a line-growing algorithm as proposed by Förstner (1994) within ± 25 pixels extended bounding box of the building model. The extracted image lines were filtered out by applying three thresholds parallel threshold, buffer size and minimum overlap. This determines the number of extracted image match lines per model line. All the match lines together give a tentative building outline in the image space per image.

3. How can the building outlines detected in aerial images be used to improve the eave and gutter sides of the 3D models?

   The building outlines determined based on the model-image line matching, were used for 3D building refinement processes. This was done in two steps. In the first step, shift per model line was estimated by fitting the model line to the matched image lines. Thus estimated shift values are in image space and they are recalculated for 3D space of the model. Eave adjacency constraints, gutter adjacency constraints and gutter symmetry constraints were exploited while recalculating the shift value in 3D object space. In the second step, the 3D models were adjusted geometrically maintaining its topology. In this process, shift values were checked to determine whether the eave or gutter side roof plane needs to extend or trim. Then the 3D roof planes were extended or trimmed to reach matched image line as suggested by shift values. This was done for eave lines, gutter lines, ridge lines and interior roof intersection lines maintaining its 3D roof topology and roof orientation as of the input models.

4. How can the improvement of the eave and gutter sides of the building be judged?

   One of the method to judge the improvement of the eave/gutter sides of the building is visual inspection. It was done by projecting the adjusted 3D models in the image space with known interior and exterior orientation parameters. Then planimetric and 3D distances were computed between the object coordinates of adjusted 3D models and input models. The maximum ranges of adjusted 2D and 3D shift values were assessed. Finally, the adjusted 3D models were evaluated as described in (Rottensteiner et al., 2012).

5. Which methods should be used to test the developed algorithm?

   Adjusted 3D models were projected in the image space and checked by visual inspection. Later, input models and adjusted models are evaluated with the external ISPRS benchmark reference dataset (Rottensteiner et al., 2012). In the evaluation method, the focus is on the quality of the roof plane segmentation and on the geometrical accuracy of the roof polygons. In the geometrical errors assessment, RMS errors is determined for the planimetric distances of the extracted roof plane boundary points to their nearest neighbours on the corresponding reference boundaries. The RMS in height difference(RMSZ) is determined by comparing two synthetic DSMs generated from the 3D building models. The RMSZ is the height difference between the reference planes and the all corresponding extracted planes. The RMS and RMSZ values obtained for adjusted models assessment are lesser than the input models. This shows the developed algorithm can improve the 3D models obtained from lidar data.

5.3 RECOMMENDATIONS

For the further improvement in the method and 3D building models, some of the recommendations of this study are listed below.

- There is still a problem in obtaining good building outline when the images have bad background contrast. Images from varying viewing angle will be fruitful to overcome this case. The conflict in eave adjacency constraint can be avoided if we could get corresponding image line of the building outline.
- Gutter symmetry is determined based on the input model geometry and exploited to refine the 3D models. The threshold applied for checking gutter symmetry may not suffice to determine the symmetry for all models. This needs to consider the characteristics of the matched as well as other longer length extracted image lines.
- 3D building models are adjusted geometrically by applying the main three constraints eave adjacency, gutter adjacency and gutter symmetry. Conflict between them is observed. To sort out, it is recommended to use constrained Least Square Adjustment (LSA) where constraints can be put as observations and can be rejected.
- One of the assumption made in 3D building adjustment is input models have to be correct topology. For this case, either input models must have correct topology or algorithm needs to be extend for improving the 3D models with incorrect topology.
- The 3D model lacks from small structure like chimney. Chimney construction can be done by exploiting the information from high resolution aerial image and lidar data to get more detailed 3D models.
- Roof texture mapping is seen as essential for realistic visualization of the 3D models. Proper texture from aerial image can be projected into corresponding the roof planes to make more realistic 3D models.

Bibliography

Ackermann, F. (1999). Airborne laser scanning-present status and future expectations. *ISPRS Journal of Photogrammetry and Remote Sensing*, 54(2):64–67.

Akca, D., Freeman, M., Gruen, A., Sargent, I., and Grün, A. (2008). *Quality assessment of 3D building data by 3D surface matching*. Institute of Geodesy and Photogrammetry, ETH Zurich.

Baltsavias, E. P. (1999). A comparison between photogrammetry and laser scanning. *ISPRS Journal of Photogrammetry and Remote Sensing*, 54(2-3):83–94.

Bonett, D. G. and Price, R. M. (2002). Statistical inference for a linear function of medians: Confidence intervals, hypothesis testing, and sample size requirements. *Psychological Methods*, 7(3):370–383.

Brenner, C. (2004). Building reconstruction from images and laser scanning. *International Journal of Applied Earth Observation and Geoinformation*, 6(3-4):187–198.

Burns, J. B., Hanson, A. R., and Riseman, E. M. (1986). Extracting straight lines. *Pattern Analysis and Machine Intelligence, IEEE Transactions on*, PAMI-8(4):425–455.

Cramer, M. (2010). The DGPF-Test on Digital Airborne Camera Evaluation Overview and Test Design. *Photogrammetrie-Fernerkundung-Geoinformation*, 2010(2):73–82.

Csathó, B., Schenk, T., Lee, D., and Filin, S. (1999). Inclusion of multispectral data into object recognition. *International Archives of Photogrammetry and Remote Sensing*, 32:part 7–4–3.

Dal Poz, A., de Souza Correia, L., Fazan, A., Marcato, V., and Simonsen, R. (2009). 3D lidar building roof refinement using photogrammetric data. In *International Cartography Conference (24th ICC)*, Santiago.

Förstner, W. (1994). A framework for low level feature extraction. *Computer Vision - ECCV' 94*, pages 383–394.

Förstner, W. (1999). 3D-city models: Automatic and semiautomatic acquisition methods. *In: D. Fritsch and R. Spiller(eds), Photogrammetric Week 99, Wichmann Verlag*, pages 291–303.

Fua, P. (1996). Model-based optimization: Accurate and consistent site modeling. *International Archives of Photogrammetry and Remote Sensing*, 31:222–233.

Haala, N., Hastedt, H., Wolf, K., Ressl, C., and Baltrusch, S. (2010). Digital photogrammetric camera evaluation generation of digital elevation models. *Photogrammetrie-Fernerkundung-Geoinformation*, 2010(2):99–115.

Habib, A., Shin, S., and Morgan, M. (2002). Automatic pose estimation of imagery using free-form control linear features. *International Archives of Photogrammetry Remote Sensing and Spatial Information Sciences*, 34(3/A):150–155.

ISPRS (2012). Web site of the ISPRS test project on urban classification and 3d building reconstruction. http://www.itc.nl/ISPRS_WGIII4/tests_datasets.html, (07/02/2012).

Kaartinen, H., Hyyppä, J., Gülch, E., Vosselman, G., Hyyppä, H., Matikainen, L., Hofmann, A., Mäder, U., Persson, ., and Söderman, U. (2005). Accuracy of 3D city models: EuroSDR comparison. *International Archives of Photogrammetry, Remote Sensing and Spatial Information Sciences*, 36(3/W19):227–232.

Lee, D. H., Lee, K. M., and Lee, S. U. (2008). Fusion of lidar and imagery for reliable building extraction. *Photogrammetric Engineering and Remote Sensing*, 74(2):215–225.

Li, S. (1994). *Markov random field models in computer vision*, volume 801 of *Lecture Notes in Computer Science*, pages 361–370. Springer Berlin / Heidelberg.

Lowe, D. G. (1991). Fitting parameterized three-dimensional models to images. *Pattern Analysis and Machine Intelligence, IEEE Transactions on*, 13(5):441–450.

Ma, R. (2004). *Building model reconstruction from lidar data and aerial photographs*. PhD thesis, The Ohio State University, Ohio, USA.

Maas, H.-G. and Vosselman, G. (1999). Two algorithms for extracting building models from raw laser altimetry data. *Isprs Journal of Photogrammetry and Remote Sensing*, 54(2-3):153–163.

Oude Elberink, S. (2009). Target graph matching for building reconstruction. *In: Proceedings of Laser scanning '09 : ISPRS Vol. 38 prt 3/W8, 1-2 September 2009, Paris, France. / ed. by. F. Bretar, M. Pierrot-Deseilligny and M.G. Vosselman. ISPRS, 2009. pp. 49-54.*

Oude Elberink, S. (2010a). *Acquisition of 3D topgraphy : automated 3D road and building reconstruction using airborne laser scanner data and topographic maps*. PhD thesis, University of Twente, Faculty of Geo-Information Science and Earth Observation (ITC), Enschede.

Oude Elberink, S. (2010b). Quality measures for building reconstruction from airborne laser scanner data. *International Archives of Photogrammetry, Remote Sensing and Spatial Information Sciences*, 38(Part 3A):198–203.

Oude Elberink, S. and Vosselman, G. (2009). Building reconstruction by target based graph matching on incomplete laser data: Analysis and limitations. *Sensors*, 9(8):6101–6118.

Oude Elberink, S. and Vosselman, G. (2011). Quality analysis on 3d building models reconstructed from airborne laser scanning data. *ISPRS Journal of Photogrammetry and Remote Sensing*, 66(2):157–165.

Panday, U. S. (2011). Fitting of parametric building models to oblique aerial images. Master's thesis, University of Twente, Faculty of Geo-Information and Earth Observation (ITC), Enschede.

Rottensteiner, F. (2006). Consistent estimation of building parameters considering geometric regularities by soft constraints. *International Archives of the Photogrammetry, Remote Sensing and Spatial Information Sciences*, 36(3):13–18.

Rottensteiner, F. (2011). Isprs test project on urban classification and 3d building reconstruction: Evaluation of building recpnstruction results. *Submitted to ISPRS, Commission III, WG III/4.*

Rottensteiner, F., Sohn, G., Gerke, M., Baillard, C., Benitez, S., and Breitkopf, U. (2012). The ISPRS benchmark on urban object classification and 3D building reconstruction. *Submitted to ISPRS, Commission III, WG III/4*.

Rutzinger, M., Rottensteiner, F., and Pfeifer, N. (2009). A comparison of evaluation techniques for building extraction from airborne laser scanning. *Selected Topics in Applied Earth Observations and Remote Sensing, IEEE Journal of*, 2(1):11–20.

Sester, M. and Förstner, W. (1989). Object location based on uncertain models. *Mustererkennung 1989*, pages 457–464.

Stamos, I. and Allen, P. E. (2000). 3-D model construction using range and image data. In *Computer Vision and Pattern Recognition, 2000. Proceedings. IEEE Conference on*, volume 1, pages 531–536 vol.1.

van den Heuvel, F. A. (1998). 3D reconstruction from a single image using geometric constraints. *ISPRS Journal of Photogrammetry and Remote Sensing*, 53(6):354–368.

van den Heuvel, F. A. and Vosselman, G. (1997). Efficient 3D-modeling of buildings using a priori geometric object information. *Videometrics V*, 3174:38–49.

Vosselman, G. (1998). Interactive alignment of parameterised object models to images. *International Archives of Photogrammetry and Remote Sensing*, 32:272–278.

Vosselman, G. (2002). Fusion of laser scanning data, maps, and aerial photographs for building reconstruction. In *IEEE International Geoscience and Remote Sensing Symposium (IGARSS 2002)/24th Canadian Symposium on Remote Sensing*, volume 1, pages 85–88.

Wang, S. and Tseng, Y. (2002). Image orientation by fitting line segments to edge pixels. In *Asian Conference on Remote Sensing(ACRS)*, volume 2002.

Zlatanova, S. and van den Heuvel, F. A. (2002). Knowledge-based automatic 3d line extraction from close range images. *International Archives of Photogrammetry Remote Sensing and Spatial Information Sciences*, 34(5):233–240.